NASA CR-145168

DEVELOPMENT OF THE TECHNOLOGY FOR THE FABRICATION OF RELIABLE LAMINAR FLOW CONTROL PANELS

February, 1977

By L. E. Meade, A. O. Kays, R. S. Ferrill and H. R. Young

Prepared under Contract No. NAS 1-14409 by
LOCKHEED-GEORGIA COMPANY
Marietta, Georgia

for

NASA
Langley Research Center
NATIONAL AERONAUTICS AND SPACE ADMINISTRATION

FOREWORD

This Final Technical Report describes the contract work performed from April 1976 through September 1976, and is submitted in fulfillment of the requirements of Contract NAS 1-14409. This contract was conducted under the sponsorship of the Materials Application Branch of the Materials Division of the NASA Langley Research Center. Mr. William E. Howell, Composites Section, was the NASA project monitor. Mr. L. E. "Roy" Meade was the Lockheed-Georgia Program Manager.

Major contributions to the work described herein were provided by the following Lockheed-Georgia personnel:

Flight Sciences	R. S. Ferrill H. R. Young
Aerodynamics	J. A. Bennett
Materials and Processes	A. O. Kays *
Fabrication	R. T. Beall
Testing	J. R. Warnick (airflow) W. M. McGee (material strength)
LFC System Consultation	R. F. Sturgeon

*Deputy Program Manager

This report is also identified as LG77ER0081 for Lockheed-Georgia Company internal control purposes.

ABSTRACT

A program was conducted to assess materials and develop fabrication techniques for use in the manufacture of wing surface materials compatible with the application of laminar flow control to subsonic transport aircraft. Materials investigated included both aluminum alloys and nonmetallic composites. The concepts investigated included perforations and slots in the metallic test panels and microporosity and perforations in the composite test panels. Perforations were produced in the metallic test panels by the electron beam process and slots were developed by controlled gaps between the metal sheets. Microporosity was produced in the composite test panels by the resin bleed process, and perforations were produced by the fugitive fiber technique. Each of these concepts was fabricated into test panels, and air flow tests were conducted on the panels. Flow test results for each material specimen were compared with an analytically predicted variable suction criteria, and indicated acceptable performance for all but the microporous composite specimens. Contamination and cleaning tests were conducted on selected electron beam perforated panels. Maximum increases in pressure loss due to contamination of 23 percent were observed, and in general the cleaning process successfully removed the contaminant. Further flow analysis included flow friction factor evaluation with good data consolidation for all test conditions of electron beam perforations and slotted test panels. Several samples of the perforated composite panels were submitted to NASA along with material data sheets.

CONTENTS

CONTENTS (Continued)

LIST OF FIGURES

LIST OF FIGURES (Continued)

LIST OF FIGURES (Continued)

LIST OF TABLES

ABBREVIATIONS AND SYMBOLS

Abbreviation/ Symbol	Description
cm	Centimeter
D	Hole diameter
EB	Electron beam
f	Empirical friction factor
ft	Foot
g_c	Gravitational constant, $kgm/N\ sec^2$
h	Slot length
kg	Kilogram
in	Inch
lbf	Pound force
lbm	Pound mass
LFC	Laminar Flow Control
m	Meter
$\dot{m}$	Mass flow rate
N	Newton (force)
N/m^2	Newton's per square meter (pressure)
psi	Pounds per square inch
ΔP_T	Pressure loss across test sample from upper to lower reservoirs
ΔP	Pressure loss from the still upstream reservoir to a distance, X, from the hole or slot entrance
Re_D	Reynolds number based on hole diameter = $\frac{\rho VD}{\mu}$
Re_W	Reynolds number based on slot width = $\frac{\rho VW}{\mu}$

ABBREVIATIONS AND SYMBOLS (Continued)

Abbreviation/ Symbol	Description
R_K	Roughness Reynolds number
S	Slot
t	Test Sheet thickness
V	Average velocity through a hole or slot
W	Slot width
β	Friction factor flow parameter equal to $\frac{4t}{D\ Re_D}$ for holes and equal to $\frac{t}{W\ Re_W}$ for slots
μ	Absolute air viscosity
ρ	Average static density of the air through a hole or slot
σ	Ratio of air total density at the flow entry side of the specimen to air density at standard consitions of 101.4 kN/m^2 (14.7 psi) and 314.4°K (59°F)

DEVELOPMENT OF THE TECHNOLOGY FOR THE FABRICATION OF RELIABLE LAMINAR FLOW CONTROL PANELS

By L. E. Meade, A. O. Kays, R. S. Ferrill and H. R. Young

1.0 SUMMARY

A program was conducted to develop techniques for use in fabrication of reliable laminar flow control surface panels suitable for application to the wing covers of subsonic transport aircraft. The scope of this development program was limited to the evaluation of surface test panels fabricated from several materials and surface concepts. Analytical methods were employed to predict suction requirements and air flow rates through the surfaces that would be required to achieve laminar flow over aerodynamic surfaces of a subsonic transport aircraft.

The wing surface materials investigated included both aluminum alloys and nonmetallic composites. Aluminum alloy test panels were fabricated using the electron beam process for formation of the perforations. Aluminum alloy sheets were used in fabrication of slotted test panels by controlling the gap between the sheets. Perforations were produced in the composite test panels by the fugitive fiber techniques and microporosity was developed by the resin bleed process. Each of the aforementioned concepts was applied in the fabrication of test panels for a range of porosities. Flow tests were conducted on the test panels in a flow test facility. Flow test results for each material specimen were compared with an analytically predicted variable suction criteria, and indicated acceptable performance for all but the microporous composite concepts. Contamination and cleaning tests were conducted on selected electron-beam-perforated panels. Maximum increases in pressure loss due to contamination of 23 percent were observed, and in general the cleaning process successfully removed the contaminant. Further flow analysis included flow friction factor evaluation with good data consolidation for all test conditions of electron beam perforations and slotted test panels. Tensile strength and modulus were determined on several perforated composite panels and compared with typical properties of solid (non-perforated) panels. Several samples of the perforated composites were submitted to NASA along with material data sheets.

2.0 INTRODUCTION

Control of air flow over the aerodynamic surfaces to maintain laminar flow conditions offers excellent promise of reduced drag for aircraft performance improvement. The theoretical methods and the engineering and design techniques for the application of laminar flow control (LFC) have been reasonably well known since the mid-1940's. The validity of this laboratory background was established in the 1960 to 1966 period by the X-21A Laminar Flow Control Program (Reference 1). Although this effort provided a successful flight demonstration of LFC, the combination of LFC system weight, production cost, and potential maintenance problems resulted in a system which was not commercially competitive with aircraft using existing technology.

The major problem areas identified in the development of LFC aircraft were related to the costs associated with manufacturing and maintaining sufficiently smooth suction surfaces. At that time, the available technology would not permit consideration of other than conventional materials for LFC suction surfaces. However, progress in the definition of properties and manufacturing procedures, as well as a reduction in costs, may now permit the economical application of both composite materials and advanced metallic materials.

In previous programs, the absence of suitable porous materials or techniques for the economical perforation of surface materials constrained designs to the use of slotted LFC surfaces. Recent advances permit consideration of non-metal composite surfaces fabricated in porous or perforated configurations providing surface smoothness limited only by the mold smoothness. In addition, manufacturing procedures have been developed which allow consideration of perforated metal surfaces for an LFC aircraft on a production basis.

This program, conducted by the Lockheed-Georgia Company, was one of three similar efforts sponsored by the NASA to exploit these advances in materials and manufacturing technology in the development of procedures for use in the fabrication of reliable porous or perforated LFC surface panels compatible with the requirements of subsonic transport aircraft. The program included the following tasks:

- Task I - Laminar Flow Control Investigation
- Task II - Mechanical Property Material Evaluation
- Task III - Symposium

The program tasks and associated schedules are shown in Figure 1.

The integration of the major study tasks into the plan employed in conducting the program is shown schematically in Figure 2. Investigations conducted in the performance of all study tasks are described in Sections 3 through 5 of this report.

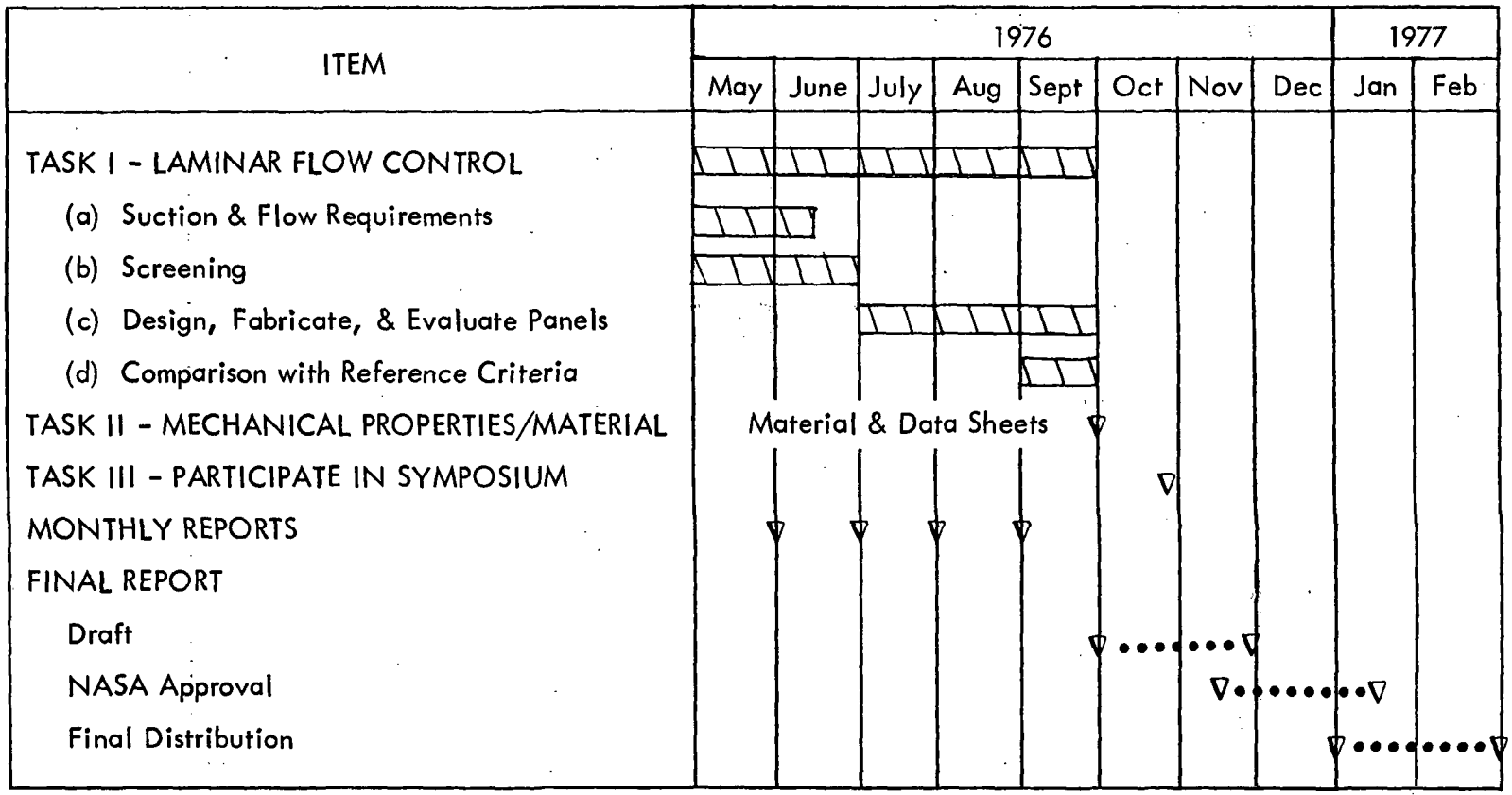

FIGURE 1. PROGRAM SCHEDULE

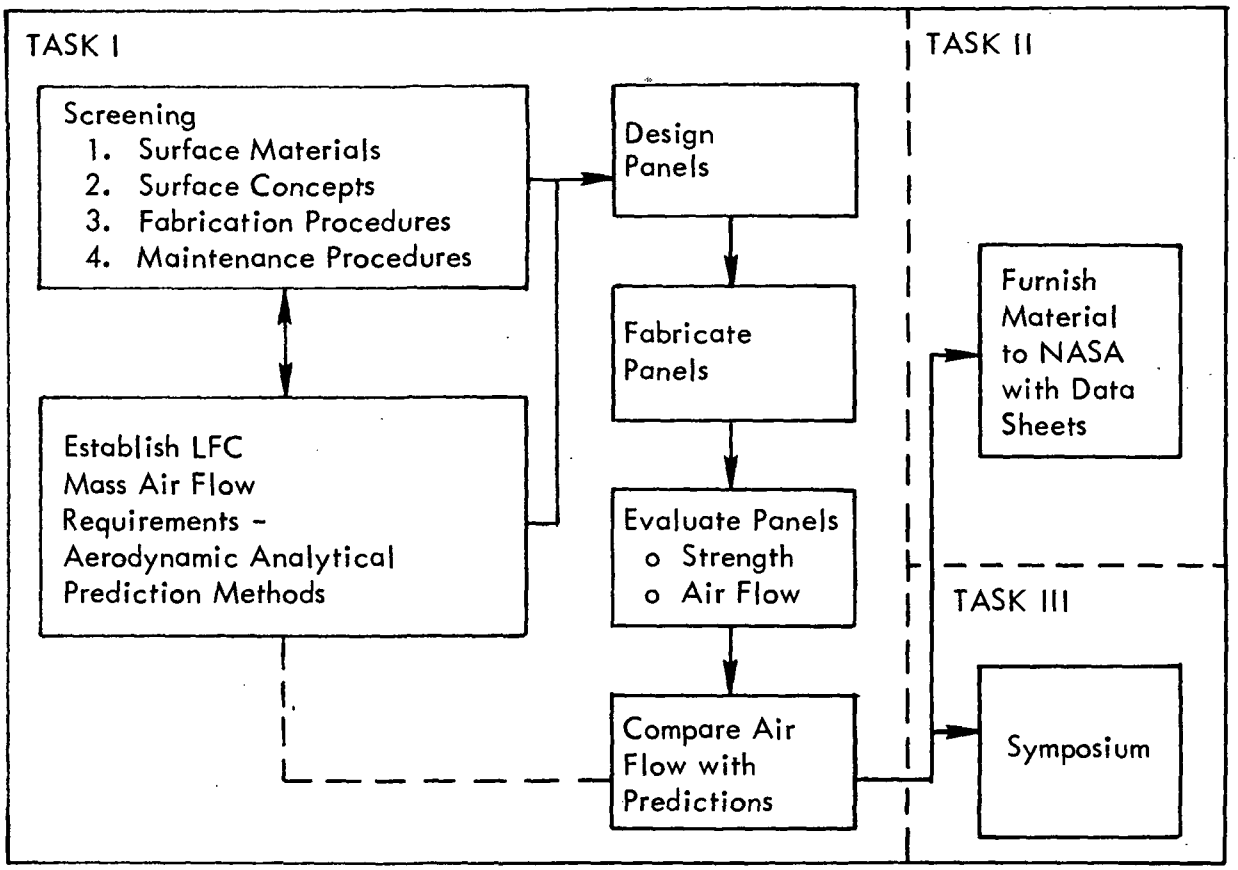

FIGURE 2. PROGRAM PLAN

3.0 TASK I - LAMINAR FLOW CONTROL INVESTIGATION

3.1 DESIGN SUCTION CRITERIA

An analytical evaluation was made to establish preliminary criteria for screening, selection, and evaluation of candidate suction surface materials and configurations. These surface materials are of three basic types: porous, perforated, and slotted. Any of these types of surfaces must ultimately provide the distributed suction flow through the surface that is required to achieve laminarization. This distributed suction must be achieved at a pressure differential across the surface that is compatible with the external surface pressures and the internal ducting pressures.

The external surface pressures are defined by the external surface aerodynamic environment, including the altitude and flight speed of the aircraft design point, the type of airfoil, the local surface pressures over the airfoil, and the local distributed suction flow required to achieve laminar flow over the surface. The requirement for uniformity of suction flow through the surface dictates that the pressure drop through the surface be maintained equal to or above a defined minimum value to limit the sensitivity of the suction flow to local surface and internal ducting pressure disturbances. On the other hand, excessively high pressure losses through the surface must be avoided since they necessitate unduly large ducting and suction pump systems. The complex nature and opposite tendency of these requirements prohibit the definition of general criteria that would satisfy all installations. Specific criteria may only be established for a single application resulting from numerous compromises. Therefore, it was not the intent of this evaluation to explore all possibilities but rather to establish criteria that would be representative and realistic for a typical application.

3.1.1 Design Point Application

The application chosen for this program was the LFC-200-S airplane configuration presented in Reference 2. This airplane, shown in Figure 3, is configured for 200 passengers with a 10,186 km (5500 nm) range at a cruise altitude of 10,668 m (35,000 ft.) and 0.8 Mach number. While this airplane and suction system employed a slotted configuration, the distributed suction requirements and surface pressure loss restrictions for it are equally applicable to porous or perforated surfaces.

The assumed surface ducting system is illustrated in Figure 4. The suction flow enters the wing through openings on the skin in the shaded areas, hereafter termed "penetrated" areas. These openings may either be in the form of pores or perforations through part or all of the penetrated areas, or in the form of discrete slots running spanwise in each of the penetrated areas. Since the suction flow may pass through the entire unobstructed porous or perforated surface area, it follows that the flow criteria for these surface configurations must be defined in terms of the suction flow per unit of penetrated area. In Figure 4, it may be seen that the substructure obstructs a portion of the suction area; therefore, the area through which the flow must enter is limited to the shaded area. It is also apparent that, if a reduction in suction flow is desired, the bands of penetrated surface may be reduced in width or the total area of penetration

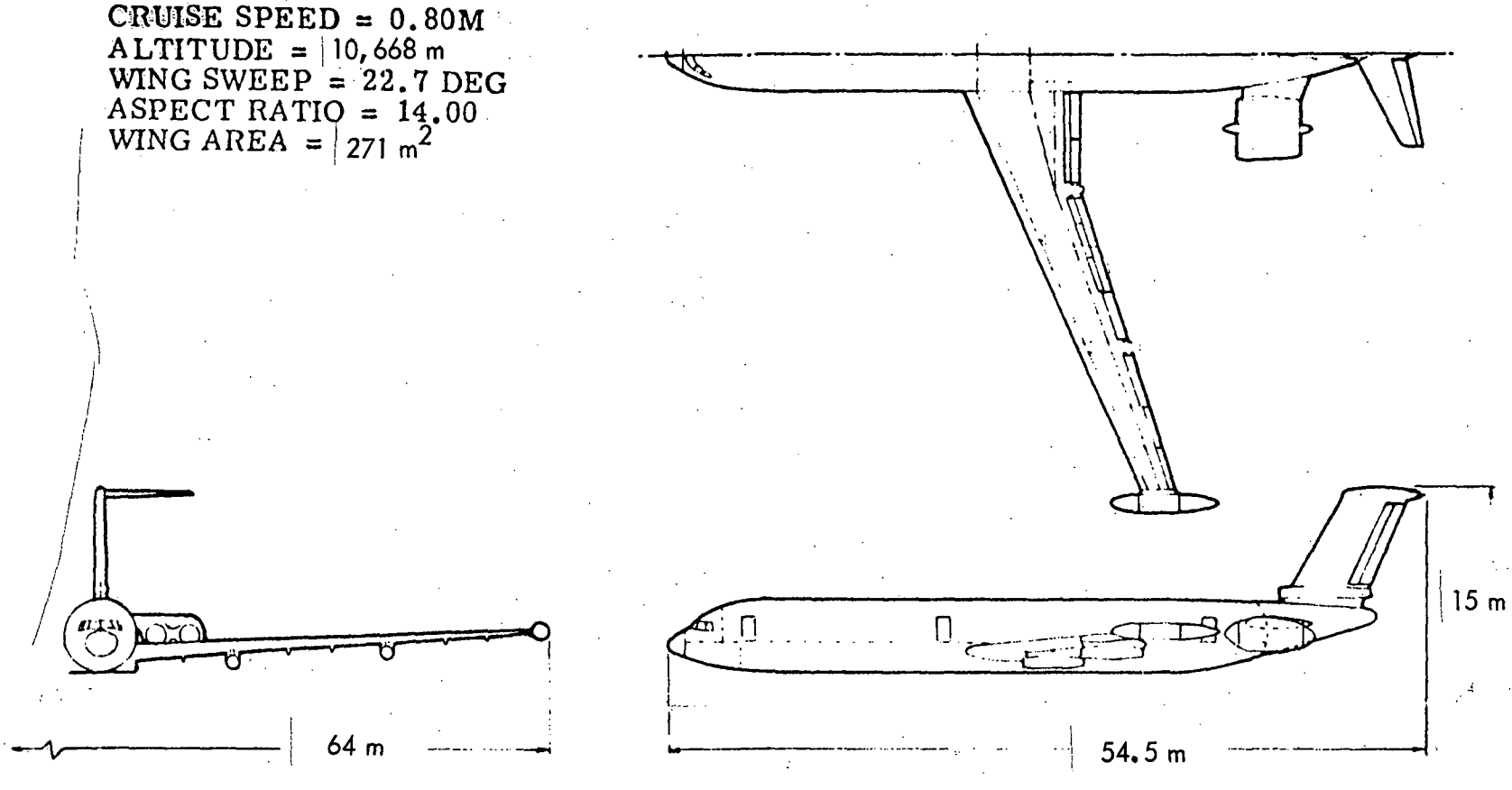

FIGURE 3. GENERAL ARRANGEMENT, INITIAL LFC-200-S BASELINE CONFIGURATION

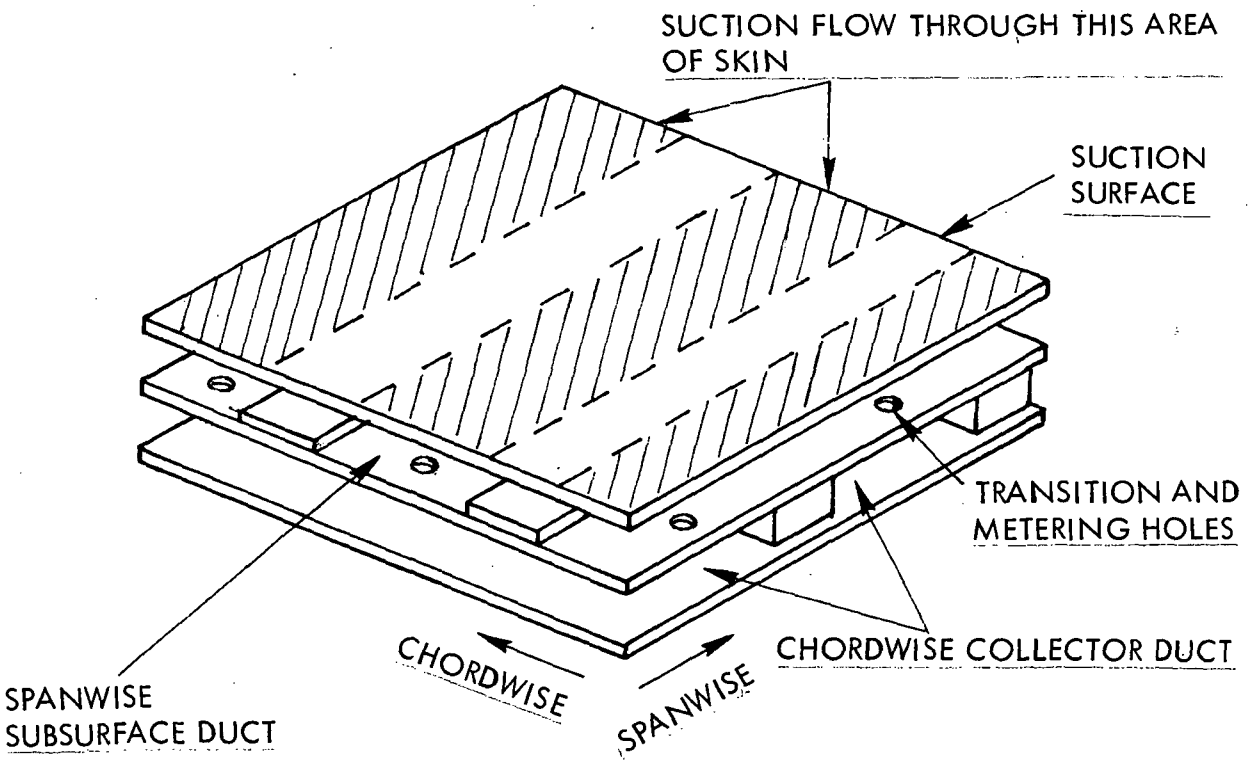

FIGURE 4. SURFACE DUCTING SYSTEM

(porosity) may be reduced. If increases in suction flow are desired, they may be achieved only at the expense of higher pressure drop through the surface or by increases in porosity. For purposes of the current reference criteria, it was assumed that 25 percent of the suction surface was obstructed by the substructure with all suction flow passing through the remaining 75 percent of the surface. If the surface penetration is in the form of slots, there may be only one slot located between the subsurface support strips. The suction flow reference criteria for slots must, therefore, be defined in terms of flow per unit slot length and adjustments in flow through the surface may be achieved by increasing or decreasing the slot width or the slot spacing. For purposes of the reference criteria established for this study, nominal slot spacing was assumed to be 5.08 cm (2 in.).

After passing through the surface, the suction flow enters the system of spanwise subsurface ducts shown in Figure 4. The spanwise flow distribution is sensitive to spanwise pressure distribution in the subsurface ducts. Air drawn into the spanwise ducts is transferred to the chordwise collector ducts through transfer holes. These transfer openings, which also function as metering orifices, are assumed to be spaced at 5.08 cm (2 in.) intervals along these ducts; thus, the maximum flow distance of suction air in the spanwise ducts is 2.54 cm (1 in.) before entering a metering hole. A maximum flow velocity of Mach 0.2 in these ducts was considered to be the upper limit to prevent an influence of acoustic disturbances on the distribution of flow through the surface. The maximum velocity in the subsurface duct of approximately Mach 0.020 was found to be necessary to prevent subsurface duct pressure losses from excessively influencing the local spanwise flow distribution through the surface. A 3 percent pressure loss lower limit through the surface passages (pores, perforations or slots), in conjunction with this low subsurface duct velocity limit, was found analytically to result in local spanwise variation of flow through the surface of approximately $\pm$ 1 percent which was considered acceptable. Actual maximum velocity in the subsurface duct was found to be in the order of Mach 0.01 for the assumed example configuration.

After passing through the metering holes, the suction flow enters chordwise collector ducts which pass across the chord of the airfoil, and the flow enters a spanwise trunk duct at the leading or trailing edge of the airfoil as illustrated by the leading edge trunk duct in Figure 5. As shown in Figure 5, the air entering through the surface at Point A sustains pressure losses in passing along the subsurface duct, through the metering orifice, B, and through the collector duct, C, and finally in the trunk duct as it flows toward the suction pump. This flow entering at A, which represents the most remote point of entry into the duct system, is subjected to the greatest pressure loss before reaching the suction pump. Therefore, it is desirable to maintain the least surface pressure drop at this point to allow the highest suction flow pressure at the pump entry. Since other locations on the surface such as Point D are not so remote from the suction unit, they would be subjected to lower ducting system pressure losses. The pressure drops through these surfaces are, therefore, generally less critical. However, extended lengths of the collector ducts, as in the case of the wing root of the LFC-200-S, may place restrictions on the surface pressure drops. In areas where this surface pressure drop is critical to the system, it is desired to maintain the drop as close as possible to the minimum value (3 percent) required for good spanwise flow distribution.

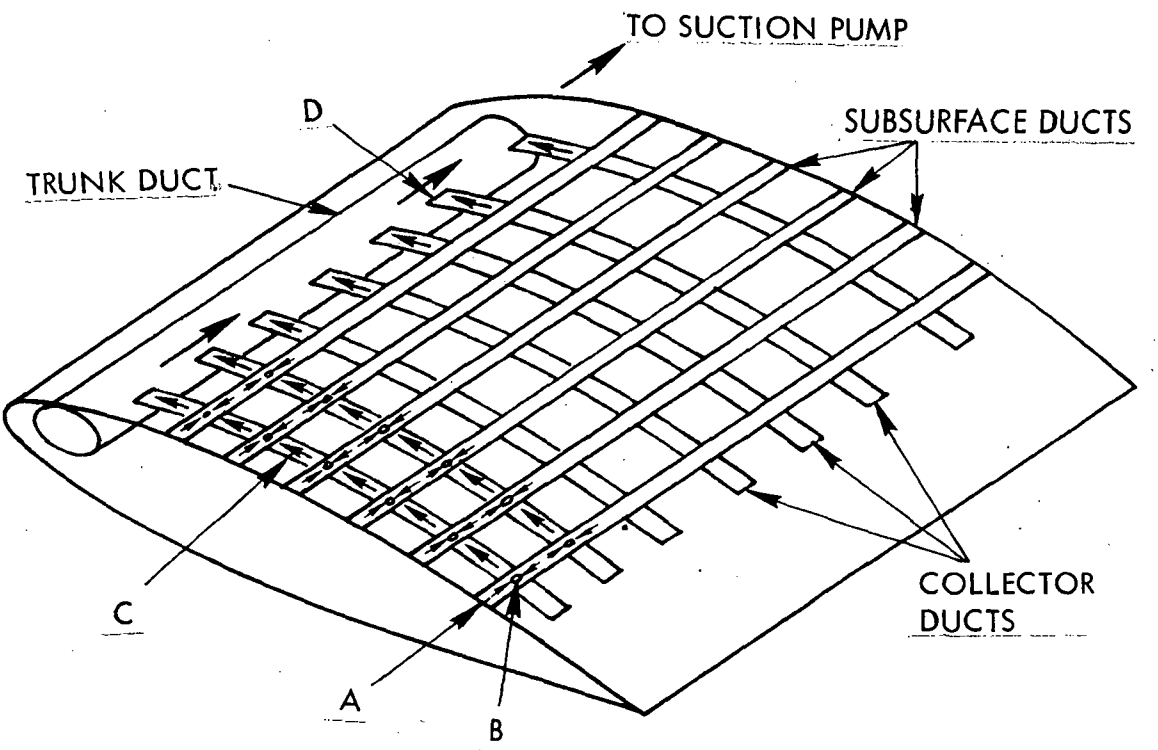

FIGURE 5. DUCTING SYSTEM

It was initially intended to conduct the evaluation of test specimens on the basis of volume flow through the surface, since this is the manner in which the suction flow requirements are usually defined. Establishment of equivalent pressure losses for testing the samples of sea level pressures at the prescribed volume flow proved to be uncertain because of the anticipated effects of flow Reynolds number in the passages through the surfaces. Therefore, the tests were modified to include simulated altitude testing. The presentation of these data resulted in a family of curves of pressure loss versus volume flow for each specific simulated altitude. This approach was subsequently abandoned in favor of an actual mass flow and normalized pressure loss, $\sigma\Delta P_T$, characteristic, where σ is the ratio of altitude density to standard sea level density. This presentation collapsed all altitude characteristics for a specimen into a single line. The surface criteria were initially determined in terms of pressure loss versus volume flow for both the altitude and equivalent sea level conditions. When the normalized characteristics were adopted, the altitude criteria were translated to $\sigma\Delta P_T$ and mass flow terms.

3.1.2 Reference Suction Criteria for Porous and Perforated Surfaces

An examination was made to determine the range of suction flow requirements for all aerodynamic surfaces assumed to be suction surfaces in the LFC-200-S airplane configuration of Reference 2. This included all suction surfaces of the wing, horizontal tail, and vertical tail. It was found that the most stringent requirements were imposed by the wing in the leading edge region, where the highest suction volume flow at the most negative surface pressures (C_p values) was required. The upper wing required moderate flows at highly negative C_p values in combination with the greatest ducting pressure losses (longest duct flow paths). The lower wing surface required the lowest suction volume flows at moderate negative C_p values.

These suction flow requirements were evaluated for the external aerodynamic conditions for flight at 0.8 Mach number at altitudes of 10,668 m and 13,716 m (35,000 and 45,000 ft.) with the internal ducting system of the LFC-200-S airplane. The resulting criteria for various points on the wing are shown for perforated and porous surfaces on Figure 6 for the leading edge, upper wing, and lower wing regions of the wing surfaces. Each region was evaluated at the points most remote from the suction units. These points were found to have the lowest allowable pressure loss in each case. The surfaces were also evaluated at the points closest to the trunk duct at both the tip and root areas of the wing span. In each case, the allowable pressure loss of the surface near the tip trunk duct was slightly higher than at the most remote points. Also, the surfaces near the trunk ducts at the wing root had the highest allowable pressure losses.

It was noted earlier that various techniques are available for matching the suction flow and surface pressure losses to the local suction flow and ducting system pressure requirements. Therefore, only the points at the highest flows and lowest suction surface pressure losses, as indicated on Figure 6, are critical for each surface. Pressure losses higher than those shown for the critical points impose additional demands on the ducting and suction pump systems, while lower pressure losses may not produce a satisfactory spanwise distribution in suction flow. Some latitude is available for achieving the flow/pressure loss requirements of the critical points by adjustment of the width or spacing of the porous or perforated strip illustrated in Figure 4, particularly in the direction

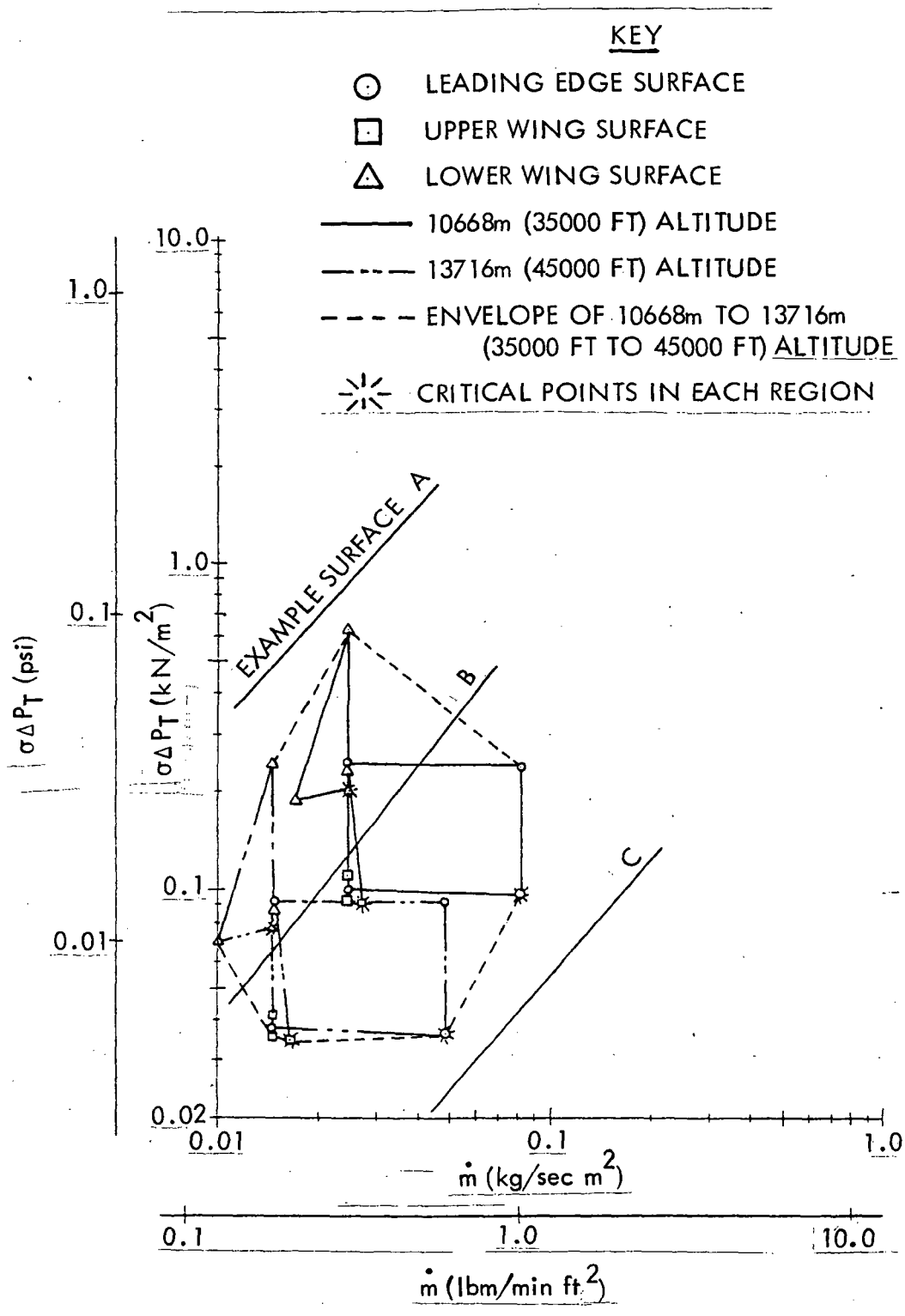

FIGURE 6. REFERENCE CRITERIA FOR POROUS AND PERFORATED SURFACES

of increasing the criteria flow at a given pressure loss. Other local requirements for higher pressure loss may be met either by further reductions in the width of the porous or perforated strip or by local restrictions to flow in the metering orifices. It is expected that restricted metering orifices would be the primary means for achieving the higher pressure losses in wing root areas and near the trunk ducts.

Example surfaces are shown on Figure 6 to illustrate acceptability of porous and perforated surface materials. Example surface A is unacceptable for any region of the wing surface, since it has low flows at all pressure losses of interest. The criteria were based on the porous or perforated material present on 75 percent of the suction surface with 25 percent of the surface blocked by substructure. Even if the extent of porous or perforated material was increased to 100 percent coverage of the suction surface, the flow criteria would be decreased only by 30 percent which would show A to be suitable for only the highest pressure loss locations. Example surface B is made suitable for the lower wing surface by reducing the width of the porous strips on the wing surface, thereby reducing the percentage of coverage on the suction surface. Again, the reference criteria are based on 75 percent coverage of the surface. If the coverage is reduced to 37.5 percent of the surface, the flow would have to pass through half the area used for the reference criteria and the criteria flow per unit area of porous material would double while maintaining the same level of pressure loss. Sample B would then meet all the lower pressure loss requirements of the adjusted lower wing criteria. The higher pressure losses would be achieved either by further reduction of the coverage or by restricting the metering orifices in the internal ducting system. Similarly, example surface C could be made suitable for meeting the requirements for the leading edge and upper wing by a reduction in surface coverage to 16 percent, but a lower porosity surface configuration with a higher percentage of surface coverage would be preferred. Again, with example C, restriction of the internal duct system metering orifices would be required for the areas requiring higher pressure loss.

3.1.3 Reference Suction Criteria for Slotted Surfaces

A similar analysis of a slotted surface configuration was made and the slot reference criteria are shown on Figure 7. The flow required through each discrete slot is dependent on the slot spacing. For purposes of establishing these criteria, a 5.08 cm (2 in.) slot spacing was assumed. The mass flow requirements were based on slot length rather than surface area as was used for the porous and perforated materials. The distributions of suction flow and required pressure losses were similar to those for the porous and perforated surfaces with the same critical wing surface locations. Limited increases and decreases in pressure loss flow requirements may be achieved by increasing or decreasing the slot spacing from the assumed 5.08 cm (2 in.) spacing. Further adjustment may be made to the metering orifices of Figure 5 to achieve pressure losses above the critical levels as in the case of porous and perforated surfaces.

Example slots are shown on Figure 7 to illustrate acceptability of slot configurations. Example slot A is unacceptable for any application due to low flows at all pressure loss levels of interest. The reference criteria are based on a spacing of 5.08 cm (2 in.), but this spacing could be reduced to 2.54 cm (1 in.) which approximates the

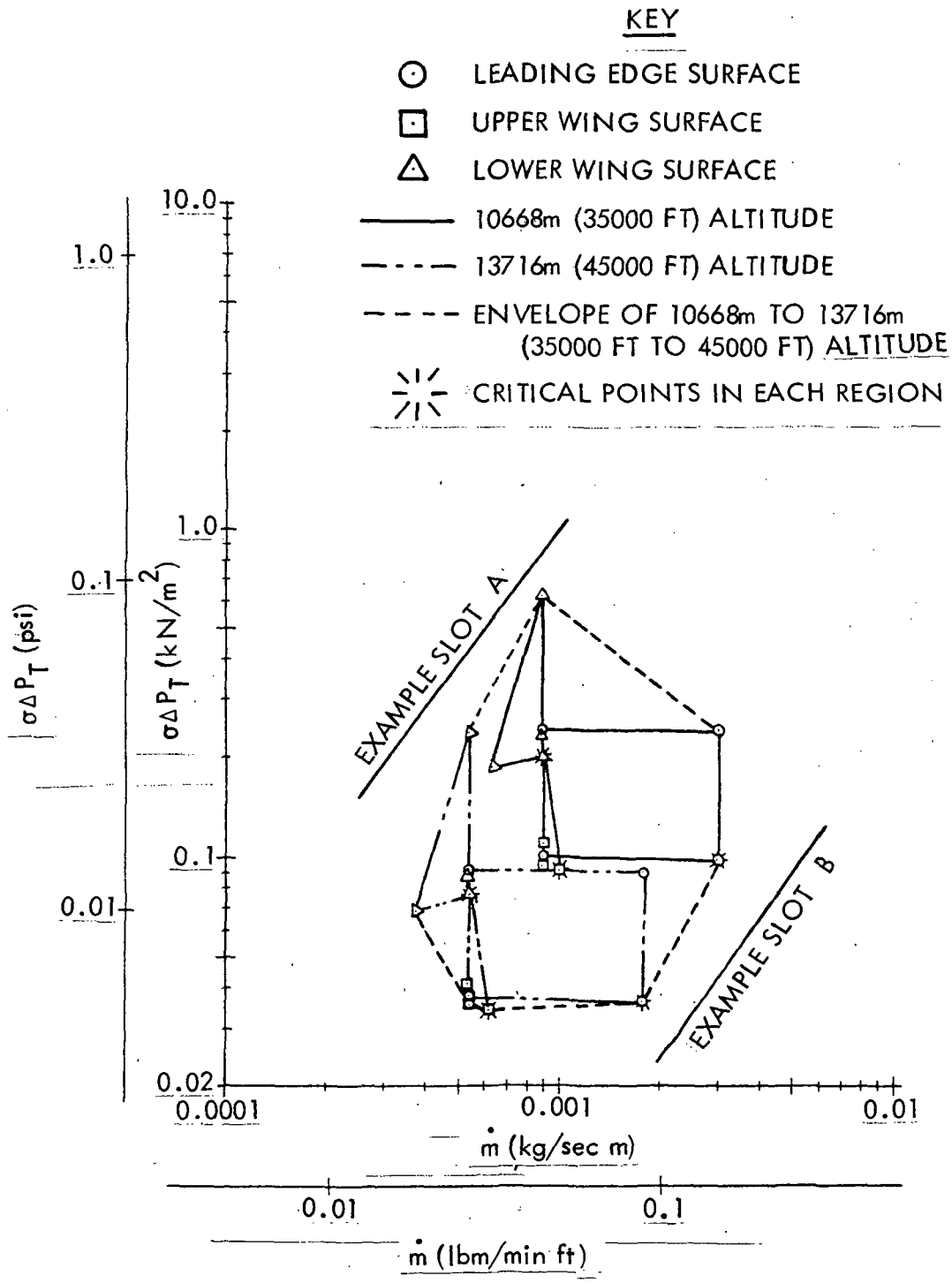

FIGURE 7. REFERENCE CRITERIA FOR SLOTS

lower limit of practical spacing. This would displace the criteria to a 50 percent lower flow, indicating that example A is still unsuitable for any but the highest pressure loss conditions. Example slot B produces an excessive flow at the critical pressure losses but could be matched to the requirements by increasing the spacing. This would necessitate a higher required flow through each slot, thereby displacing the criteria to a higher flow and a match with the sample slot flow/pressure loss could be achieved. As in the case with the porous and perforated surfaces, internal ducting metering orifices would require restriction to match the highest pressure losses.

For consistency and economy of fabrication, it is desirable to standardize the size and configuration of the suction opening (microporous, perforated, or slot) for an entire region (i.e., leading edge, upper and lower wing surface). The particular configuration is selected based on the most critical points for each region. Variations in suction flow and pressure loss required by other points in that region are then controlled by varying spacing of openings and by sizing of orifices in the ducting system. Standardization may also be necessitated with the slot configuration because of constraints on the minimum slot width that can be manufactured on a production basis within acceptable tolerances. As was noted earlier, these requirements are tailored to the specific airplane and internal ducting system selected as reference for this study. For this reason, these criteria are only typical and representative and should not be construed as specifically applicable for all LFC airplane requirements. To simplify these criteria for use in the presentation of test data, an envelope has been drawn around all data for the 10,668 m to 13,715 m (35,000 ft. to 45,000 ft.) altitudes as shown in Figures 6 and 7.

3.2 SURFACE SMOOTHNESS CRITERIA

Criteria for initial surface smoothness and waviness for LFC surfaces have been established as determined and published in Reference 2, and shown in Table I.

Only the 3-dimensional roughness requirements of Table I are applicable to the present contract. The value of 0.013 cm (0.005 in) shown in this table is based on a critical roughness Reynolds number, R_k, of 200, and therefore represents the most stringent requirement at the design altitude.

The variation of R_k with Reynolds number, airfoil section, and element fineness ratio has been measured by a number of investigators. The accumulated experimental data are summarized in References 3 and 4 and indicate that values of R_k as great as 600 are appropriate for isolated two- and three-dimensional roughness elements. Figure 8 illustrates the variation of permissible roughness height with altitude for R_k values of 200, 400, and 600 for the study airfoil at the 2% chord location. As illustrated by this figure, if $R_k = 600$ is assumed, the permissible roughness height at the design altitude increases to 0.022 cm (0.0088 in) from the 0.013 cm (0.005 in) value corresponding to $R_k = 200$.

TABLE I - SURFACE SMOOTHNESS AND WAVINESS REQUIREMENTS

LFC Surface Smoothness Requirements

Steps

- o Forward-facing Chordwise 0.033 cm (0.013 in.)
- o Aft-facing Chordwise 0.018 cm (0.007 in.)
- o Spanwise 0.033 cm (0.013 in.)

Gaps

- o Chordwise or Spanwise 0.269 cm (0.106 in.)

3-Dimensional Roughness 0.013 cm (0.005 in.)

LFC Surface Waviness Requirements

Chordwise

Wave Length		Double Wave Amplitude			
		Single		Multiple	
m	ft.	cm	in.	cm	in.
0.15	0.5	0.0254	0.010	0.008	0.003
0.30	1.0	0.0356	0.014	0.0127	0.005
0.61	2.0	0.0483	0.019	0.0152	0.006
0.91	3.0	0.0584	0.023	0.0203	0.008

Spanwise

Double Chordwise Values

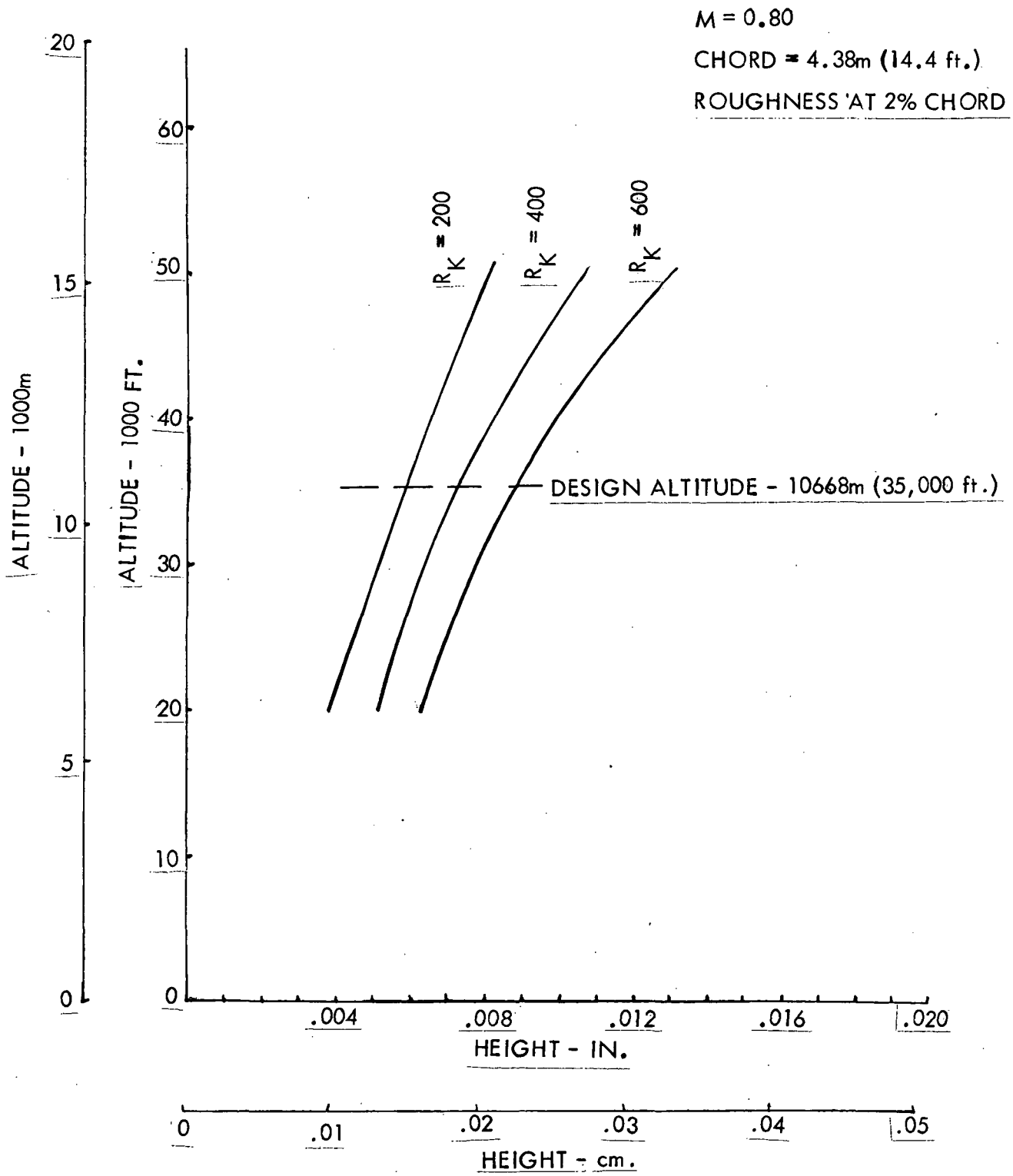

FIGURE 8. VARIATION OF ALLOWABLE ROUGHNESS WITH ALTITUDE

3.3 MECHANICAL PROPERTY REQUIREMENTS

From the previous LFC systems study of Reference 2, material requirements were based upon the glove panel face sheet being nonstructural with respect to basic wing structure loads. Therefore, the LFC surface materials were selected on the basis of requirements for tensile and compressive strengths in the 34 to 69 MN/m^2 (5,000 - 10,000 lb/in^2) range and in-plane shear strength approximately 15 to 30 percent of the tensile strength.

3.4 MATERIALS AND PROCESSES

3.4.1 Surface Materials and Concepts

3.4.1.1 Industry Survey - The industry survey for materials and concepts suitable for porous surface panels for LFC application included literature searches and contacts with materials and equipment suppliers. Literature searches were initiated through Lockheed's Scientific and Technical Information Libraries. Lockheed's Dial-a-Log system of data search includes NASA SCAN, Defense Documentation Center, Defense Materials Information Center, IDEP, and National Technical Information Service, as well as all libraries of the various Lockheed Companies. This literature search produced data on porous materials, porous plastics, acoustic or noise suppression materials, filtration materials, and leather-like materials. Several leather-like materials patents from that search were reviewed. Most of those patents were concerned with elastomeric-type materials and were not applicable to LFC materials because the mechanical properties were too low or the porosity was insufficient to allow the required air flow. Therefore, further consideration was not given to leather-like materials. Another of the porous materials from the literature search was sintered metal wire and, therefore, too heavy for consideration. Other concepts were very similar to foams and did not meet the mechanical property requirements. Several concepts for creating microporous composites were revealed, such as various blowing agents and resin staging techniques.

Contacts with materials and equipment suppliers revealed the availability of the electron beam process for perforating metals, concepts for microporous plastics (non-reinforced), and fibers and solvents used in the fugitive-fiber process.

This industry search aided in providing data and background required for selecting the surface materials and concepts used in this program and discussed in the following two subsections.

3.4.1.2 Surface Materials - The materials investigated for producing the porous surface panels in this program included both metals and composites. The metals were aluminum and titanium alloys. The composites were graphite/epoxy and Kevlar 49 (high modulus organic fiber)/epoxy. The graphite/epoxy composites included both the mat and fabric forms. The Kevlar 49/epoxy was investigated in only the fabric form. The graphite mat was Union Carbide's VMA/3066 using the pitch precursor fiber. It was impregnated with an epoxy resin. Two graphite fabric/epoxy materials were investigated. One was Fiberite HMF330C/34 prepreg using the W133 style T300 graphite fabric and X934 epoxy resin, which cures at 450°K (350°F). The other was Fiberite

HMF134/48A prepreg using the W134 style T300 graphite fabric and X48A epoxy resin, which cures at 394°K (250°F). The Kevlar 49/epoxy was Narmco Kevlar 49/5209 with 281-style Kevlar 49 fabric and 5209 epoxy resin, which cures at 394°K (250°F).

3.4.1.3 Surface Concepts - Four concepts investigated for porous surface panels were:

- o Microporous Composites
- o Perforated Composites
- o Perforated Metal
- o Slotted Metal

The microporous composite panels were fabricated by a combination of resin staging and resin bleeding and are discussed in subsection 3.4.2.1. Perforated composite panels were produced by the fugitive fiber process and are described in subsection 3.4.2.2. Perforated metal panels were manufactured by the electron beam process and are discussed in subsection 3.4.2.3. Slotted panels were produced by controlling the gap between two or more metal sheets and are described in subsection 3.4.2.4.

3.4.2 Fabrication of Porous Test Panels

3.4.2.1 Microporous Composites - Seven 12.7 by 25.4 cm (5 by 10 inches) microporous panels were fabricated by varying the resin stage, bleeder system, and pressure during cure of the panels. Table II identifies these test panels, the pertinent variables, and the figure which depicts flow test performance. Panels number MPC101, MPC102, and MPC103, where both the resin staging and cure was accomplished under vacuum bag pressure only, were considerably more porous than the remaining four panels, where the resin staging and cure was accomplished under higher pressure as indicated in Table II. Figure 9 shows a cross section of panel MPC102, depicting the voids as dark areas in the mat-based microporous composites. Figure 10 shows a cross section of panel MPC103, depicting the voids as dark areas in the fabric-based microporous composites. Flow of these microporous composites is discussed in subsection 3.5.2.1.

3.4.2.2 Perforated Composites - Eighteen composite panels were perforated by the fugitive fiber process. Table III identifies these test panels, the pertinent dimensions, type of laminate material, type of fugitive-fiber, and the flow test performance figure number. The flow characteristics of these specimens are discussed in subsection 3.5.2.2.

The following panel numbering system was devised to identify several characteristics of each panel:

1st two letters . . . MF - monofilament

3rd letter . . . Filament Source - S - Stren
K - K Mart
D - du Pont

TABLE II - MICROPOROUS COMPOSITES TEST PANELS

Specimen Number	Type Material	Material Thickness (cm)	Bleeder System	Resin Stage	Cure Temperature (°K)	Cure Pressure (kN/m^2)	Performance Figure No.
MPC101	Graphite Matt/Epoxy	0.058	4 plies 120 Fg one side	30 min. @ 394°K and 98 kN/m^2 (Vac)	450	98 (Vac)	40
MPC102	Graphite Matt/Epoxy	0.058	4 plies 120 Fg both sides	45 min. @ 389°K and 98 kN/m^2 (Vac)	450	98 (Vac)	40
MPC103	Graphite Fabric/Epoxy	0.033	4 plies 120 Fg both sides	45 min. @ 389°K and 98 kN/m^2 (Vac)	450	98 (Vac)	40
MPC104	Graphite Matt/Epoxy	0.058	2 plies 181 Fg both sides	30 min. @ 394°K and 965 kN/m^2	450	482	40
MPC105	Graphite Matt/Epoxy	0.058	2 plies 120 Fg both sides	3.6°K/min heatup rate and 98 kN/m^2 (Vac) to 394°K	Same heatup rate to 450 then cure	586	40
MPC106	Graphite Matt/Epoxy	0.058	Bleed release P2 + 3 plies 120 Fg both sides	3.6°K/min heatup rate and 98 kN/m^2 (Vac) to 394°K	Same heatup rate to 450 then cure	586	40
MPC107	Graphite Fabric/Epoxy	0.033	2 plies 120 Fg both sides	3.6°K/min heatup rate and 98 kN/m^2 (Vac) to 394°K	Same heatup rate to 450 then cure	586	40

"Page missing from available version"

TABLE III - PERFORATED COMPOSITE TEST PANELS

Specimen Number	Type Laminate Material	Type Fugitive Fiber	Material Thickness (cm)	Fugitive Fiber Diameter (cm)	% Open Area	Performance Figure Number
MFS4080.65GC	Graphite/Epoxy Fabric	Nylon Monofilament	0.066	0.020	0.65	41
MFS4080.7GC					0.70	41
MFS4081.0GC					1.00	41
MFK8110.7GC				0.028	0.70	43
MFK8111.2GC					1.20	43
MFK8111.54GC					1.54	43
MFK8112.0GC					2.00	43
MFK8110.93GC					0.93	43
MFK8111.08GC					1.08	43
MFD7100.88GC				0.0254	0.88	42
MFD7101.0GC					1.00	42
MFD7101.13GC					1.13	42
MFD7100.85K	Kevlar 49/Epoxy Fabric		0.051		0.85	44
MFD7101.2K					1.20	45
MFD7100.85GC	Graphite/Epoxy Fabric		0.066		0.85	44
MFD7101.2GC					1.20	45
MFD7100.85GW			0.053		0.85	44
MFD7101.2GW					1.20	45

1st digit . . . Filament breaking strength in pounds force

2nd & 3rd digits . . . Filament diameter in mils

4th, 5th & 6th digits . . . Percent open area

Last 2 letters . . . Laminate type - K - Kevlar 49/epoxy fabric
GC - Graphite/epoxy W133 style fabric
GW - Graphite/epoxy W134 style fabric

The fugitive-fiber process* is described in general terms as follows: Composite prepreg is laid up to the desired thickness and size, sandwiched between mylar film, stitched with fugitive fiber, and cured. The fugitive fibers are subsequently leached in a suitable solvent, leaving a straight-through hole of the approximate diameter of the fugitive fiber. The 18 panels investigated in this program were fabricated by stitching the mylar-encased panels on conventional industrial sewing machines using nylon monofilament as the fugitive fiber. Economical high-rate production would most probably be done on tufting machines such as those used in the carpet industry. Figures 11 through 22 depict the fugitive-fiber processing sequence.

Complete removal of the fugitive fiber was found difficult in this process. Trials with stranded yarn and monofilament diameters less than 0.020 cm (0.008 in.) were unsuccessful. With the monofilament fiber having diameters of 0.020 cm (0.008 in.) and larger, it was found that most of the fugitive fibers were removed upon removal of the mylar separator film. The remaining fiber could be removed with an alternating immersion in concentrated hydrochloric and formic acids.

Another difficulty experienced with the fugitive-fiber process was the inability to produce consistent hole diameters. This was inherent in the stitching process used on this program. Each stitch placed two filaments (one each on needle entry and exit) in the prepreg. During cure, resin would flow between the two filaments, which might break out on filament removal, creating a hole larger than the two filament diameters, as shown in Figure 23. It may also be seen in Figure 23 that the hole spacing is not uniform, especially in the direction transverse to the stitching direction. This is caused by the inability of the sewing machine operator to follow the guidelines provided on the mylar separator sheet shown in Figure 15.

Figure 24 shows a view of the fugitive-fiber-process perforated composite panel from the needle entry side. It is noted that the needle produces a larger hole than the two holes created by the fugitive fiber; the needle used for producing these specimens was the smallest available for the machine. As the needle proceeds through the prepreg, it pushes some material through with it. During cure, the material flows back around the fiber and leaves a burr on the needle exit side. This burr was removed by sanding. Figure 25 shows this relatively smooth side of the needle exit surface. Figure 26

*A disclosure of invention was generated and processed by the Lockheed Legal Department. An Abstract of New Technology was submitted to NASA.

"Page missing from available version"

Pages 23-30

shows a cross section of the panel taken through two of the holes produced by the fugitive fiber. The hole appears to be relatively straight-sided, indicating a cylindrically shaped hole.

It is believed that most of the inconsistencies observed with the fugitive-fiber process, with respect to characteristics such as hole diameters and hole spacing, discussed above, could be alleviated by an investigation directed at other commercial processes, such as tufting, for the production of perforated composites. In addition to producing more consistent perforations, these commercial processes should result in greatly improved economics.

Trials by Farrel Corporation for perforating graphite/epoxy composite panels by the electron beam process, described in subsection 3.4.2.3, resulted in failure of the electron beam to penetrate the laminate. Evidence points toward graphite fibers completely diffusing the electron beam, thereby preventing penetration. However, Farrel Corporation indicated that, in trials they made on Kevlar 49/epoxy composites for another company, holes were produced easily. Since this information was received late in the program, electron-beam-perforated Kevlar 49/epoxy composites were not made and tested by Lockheed-Georgia Company.

An advantage of the fugitive-fiber process for producing perforations in composites, compared with electron-beam-produced perforations, is that all fibers are coated with a resin film in the fugitive-fiber process, while the electron-beam process would leave fiber ends exposed and vulnerable to moisture vapor entry.

Visual inspection of the fugitive-fiber-perforated composite panels revealed that surface roughness was obviously well in excess of typical allowables; therefore, no detailed measurements of micro-roughness were made for comparison with criteria. Considerable improvement in the fabrication process would be required before any detailed measurements on samples would be meaningful. Restricting initial LFC operation to an altitude higher than 10,668 m (35,000 ft.) would offer some improvement in micro-roughness allowables as indicated by Figure 8; however, the basic surface micro-roughness of the porous composite samples would need considerable improvement to justify a cruise altitude even as low as 13,716 m (45,000 ft.). Therefore, improved fabrication techniques and improved micro-roughness experimental transition data base are needed before the cruise altitude, as limited by meaningful micro-roughness requirements, could be chosen.

3.4.2.3 Perforated Metal - Nine 0.051 cm (0.020 in.) thick aluminum panels were perforated by the Farrel Corporation, using the Steigerwald developed electron-beam (EB) process. Table IV identifies these test panels, the pertinent dimensions and material, and the flow test performance figure number. The flow of these specimens is discussed in subsection 3.5.2.3.

The EB process for producing perforations consists basically of the following steps:

- The metal sheet is clamped on a drum over a layer of polymeric material such as silicone rubber. The drum is capable of holding sheet sizes up to 0.35 by 1.42 m (14 by 56 in.).

TABLE IV - PERFORATED ALUMINUM TEST PANELS

Specimen Number	Type Material	Material Thicknees (cm)	EB Entrance Diameter, D2, (cm)	EB Exit Diameter, D1, (cm)	Posority Relative to D1, (%)	Performance Figure No.
EB1	Al	0.051	0.03150	0.00945	0.569	46
EB2	Al	0.051	0.02212	0.01212	1.876	46 and 48
EB3	Al	0.051	0.02248	0.01232	3.858	46 and 48
EB4	Al	0.051	0.02934	0.01478	0.483	46
EB5	Al	0.051	0.02847	0.01595	1.098	46
EB6	Al	0.051	0.03327	0.01300	1.464	47
EB7	Al	0.051	0.04783	0.02532	0.984	47
EB8	Al	0.051	0.04211	0.02408	1.807	47 and 48
EB9	Al	0.051	0.04425	0.02537	3.953	47 and 48

- The drum is inserted into a vacuum chamber.
- The vacuum chamber is closed.
- A high vacuum is drawn.
- The Steigerwald gun emits numerically-controlled EB pulses which are focused on the desired spot on the work piece.
- The hole size is controlled by focusing the size of the electron beam.
- Hole spacing is determined by positioning the drum in accordance with a predetermined computer controlled hole pattern.
- As the EB liquifies the metal, the polymeric backup material vaporizes and expels the molten material from the work piece, creating the hole.

The last step in the process explains two observations made on examination of the nine perforated aluminum panels. The first observation was that the EB entry surfaces were quite rough, while the EB exit surfaces were very smooth. As the vaporized backup material pushes the molten aluminum material out of the hole, a lip of molten aluminum forms and rapidly solidifies on the surface. The second observation is illustrated in the four photomicrographs shown in Figure 27. These sections, taken through a single hole of each of four EB specimens, show that the holes are tapered. It may be theorized that the inherently high thermal conductivity of the aluminum allows a slightly larger area of the aluminum to melt than that being vaporized in the backup polymeric material. As the vapors are expelled from the parent material, they expand and create the tapered hole.

Since the holes in the EB-perforated aluminum panels were found to be tapered, the EB entrance and exit diameters were measured for each of the nine panels and tabulated in Table IV. The measurements were accomplished by use of a filar eyepiece at approximately 150X magnification. Approximately 20 measurements were made on each surface and averaged to establish the average diameters. Of the holes measured, the diameters varied within $\pm$20 percent of the nominal diameter. However, it is expected that further work will enable better tolerance control. In general, the electron beam exit hole was circular in shape, and the electron beam entrance hole was oval with a major axis approximately 10 percent larger than the minor axis.

Examination of the EB-perforated aluminum panels revealed that, in some of the panels, some of the holes appeared to be clogged even after cleaning in an Alconox solution. Further examinations revealed that some of the holes that appeared to be started did not go through the metal sheet. To determine the effective number of holes in each of the nine EB-perforated aluminum panels, a mask was made the size of the flow test area and placed on each specimen. The masked specimen was then backlighted and photographs made of each specimen. The actual number of holes for each specimen was counted and used along with the diameters previously measured to calculate the effective percent of open area. Figures 28 through 36 show the nine backlighted photographs, and approximately 40X and 160X magnifications of the EB-perforated aluminum holes are also shown.

"Page missing from available version"

Pages 34-39

For long-term durability of LFC panels placed on aircraft wings and empennages, it is expected that aluminum perforated panels would require an anodic coating. The degree to which the EB-perforated holes can be anodized uniformly is not known at this time. Work in this area would be required prior to a selection of EB-perforated aluminum panels for an LFC application.

The surface smoothness of the EB-perforated aluminum panels, measured with a Brush Clevite Surfindicator, showed a roughness height of 0.15 μm (6 μ in.) RMS, which is much smoother than required by the surface smoothness criteria discussed in Section 3.2.

Two 0.041 cm (0.016 in.) thick titanium sheets were perforated by the EB process with approximately 0.025 cm (0.01 in.) diameter holes. One major difference between the titanium and the aluminum EB-perforated sheets was that the EB entry surface of the titanium sheets was smooth, while that surface of the aluminum sheets was rough as previously discussed for the EB-perforated aluminum panels. Since the EB-perforated titanium sheets were received late in the program, flow testing or microsectioning to determine the hole shape was not conducted.

3.4.2.4 Slots - Nine aluminum panels were fabricated with slots by bonding aluminum surface sheets on a backup as shown on Figure 37. The slot widths were controlled to within ±0.0025 cm (±0.001 in.) by shimming to the desired slot width. Table V identifies the panels, type of material, material thickness, slot width, and figure in which performance can be found in subsection 3.5.2.4.

Trials for cutting slots in titanium by the EB process were unsuccessful. Since the EB beam is not a continuous stream of energy, cutting a slot must be accomplished by overlapping energy pulses. In these overlapping pulses, vaporization of the backup polymeric material does not thoroughly expel the molten material. Therefore, a clean slot was not made.

3.5 FLOW TESTING

3.5.1 Apparatus and Procedures

The principal flow parameters to be measured were pressure loss across and rate of flow through the specimen. Two test arrangements were used; the first was designed to make a quick, economical screening of pressure loss and flow of the microporous composite specimens, while the second was designed for a more detailed analysis with the capability of suction flow variation and altitude simulation.

The first test apparatus progressed through initial and improvement stages. Figure 38 shows the initial test setup, which consists of a 10.2 cm (4 in.) diameter reservoir chamber with the test specimen clamped over the opening. The reservoir was connected to a constant-flow vacuum pump which exhausted into a wet test flow meter. The pressure loss was measured with an oil manometer between the atmosphere and the reservoir. Subsequent improvements to this test setup added an upstream reservoir to give the ability to generate simulated altitude conditions by throttling the intake from atmosphere. The same vacuum pump and flow meter were used. The pressure in the upper chamber was measured with a mercury manometer. The pressure loss between reservoirs, and consequently across the test specimens, was measured with an oil manometer.

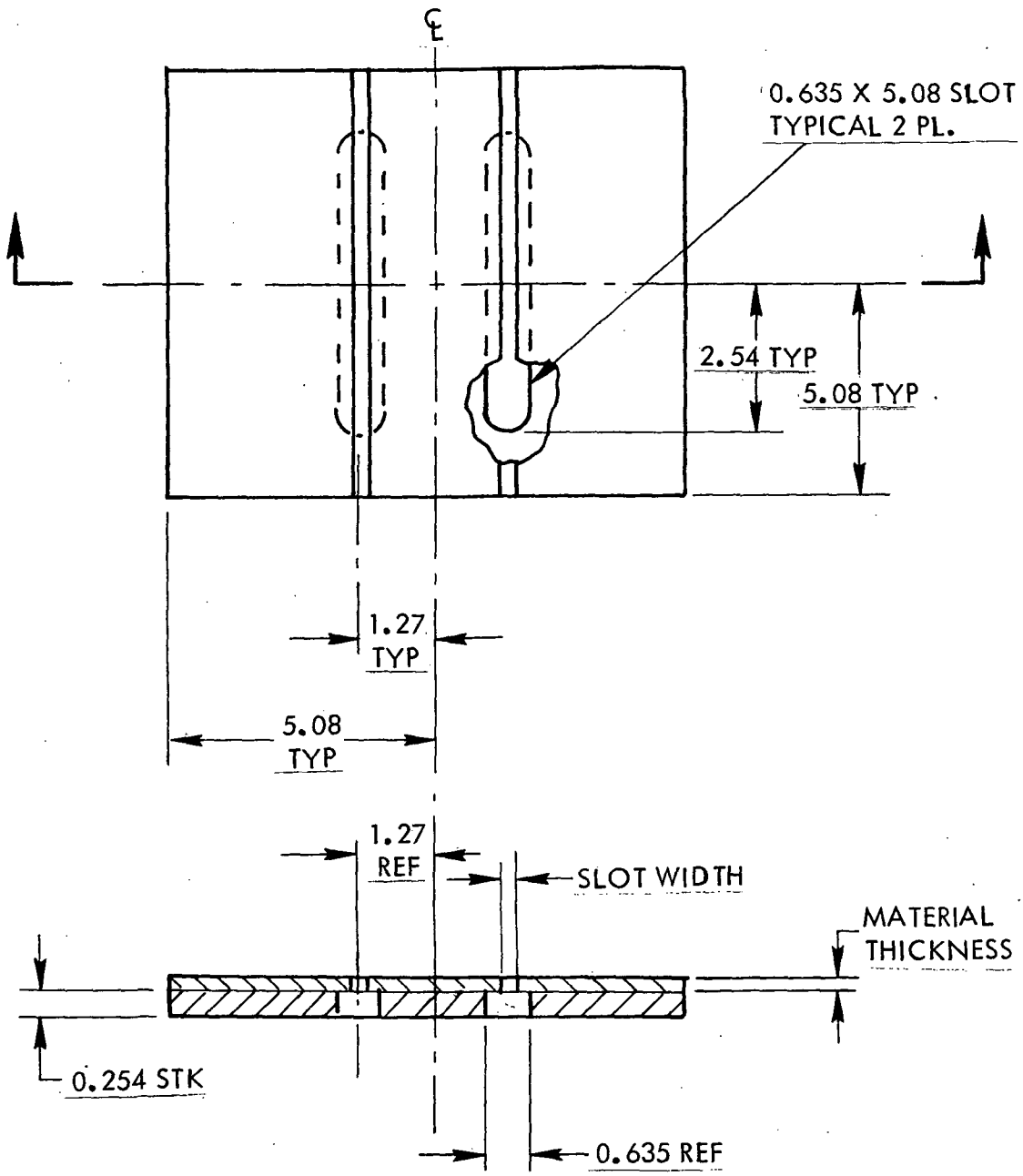

NOTE: ALL DIMENSIONS ARE IN CENTIMETERS.

FIGURE 37. SLOT TEST SPECIMEN

TABLE V - SLOTTED TEST PANELS

Specimen Number	Type Material	Material Thickness (cm)	Slot Width (cm)	Performance Figure No.
S1	Al	0.0508	0.0089	49
S2	Al	0.0508	0.0165	49
S3	Al	0.0508	0.0248	49
S4	Al	0.0508	0.0330	49
S5	Al	0.0305	0.0222	50
S6	Al	0.1016	0.0222	50
S7	Al	0.160	0.0248	50
S8	Al	0.229	0.0267	50
S9	Al	0.3175	0.0241	50

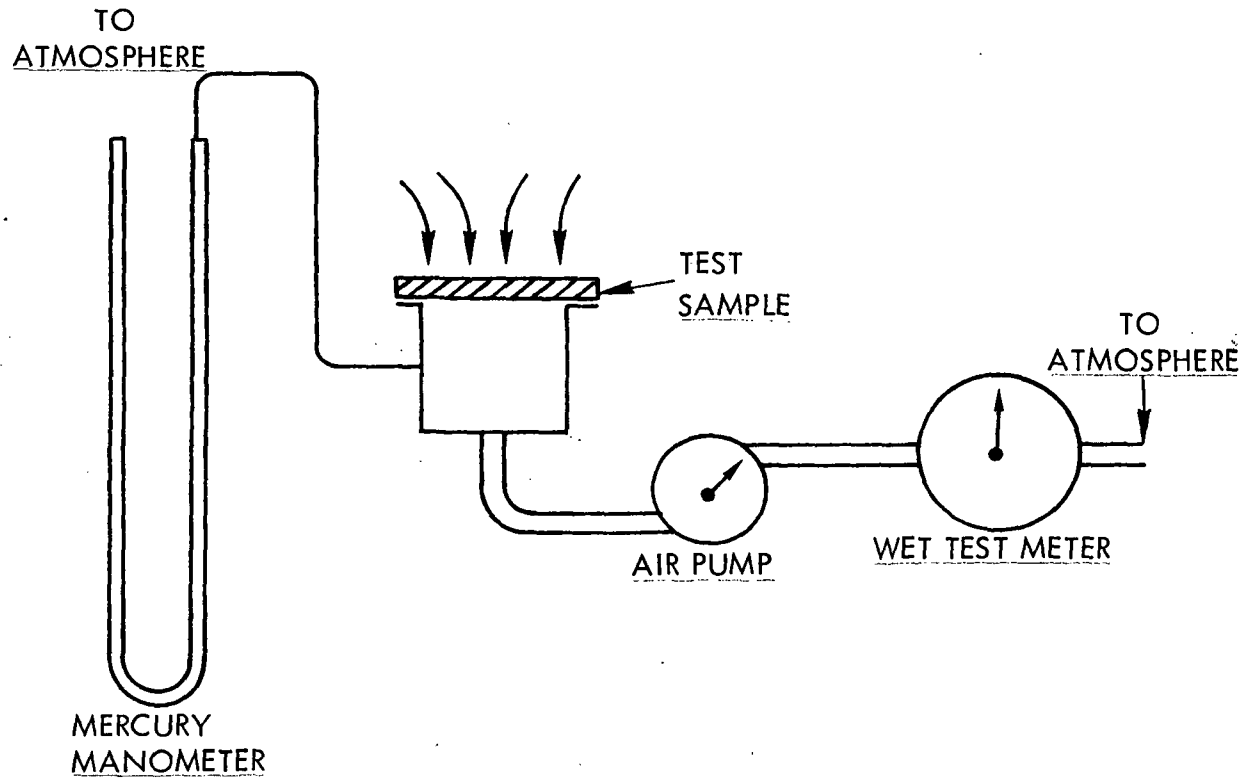

FIGURE 38. SCREENING TEST APPARATUS

The second test setup, which incorporated further improvements to enable detailed analysis, is shown in Figure 39. It was used for conducting flow tests on the perforated composites, the electron-beam-perforated aluminum, and the slotted aluminum specimens. This final apparatus is similar to the improved screening test setup, except that the reservoir diameter was reduced to 6.35 cm (2.5 in.). The vacuum source was the plant vacuum system which provided the capability of varying the flow rate. The flow was measured by means of a linear flowrater, and a thermocouple was added in the inlet to record air temperatures entering the upper reservoir. All tests were conducted at ambient temperature conditions of 291 to 340°K (65 to 85°F) with selected samples run over a wider range of temperatures to evaluate temperature effects, which are discussed in subsection 3.5.2.3. A detailed description of the test equipment is given in Appendix B.

The following test procedure was used for all flow tests:

- The test specimen was installed either by clamping it over the lower reservoir or by clamping it between the upper and lower reservoirs.
- Suction was applied to the system to induce flow and, in the case of the final test apparatus, the amount of suction flow was adjusted to the desired value.
- Where possible, as dictated by the test apparatus, the intake was throttled into the upper reservoir to generate the desired simulated altitude condition.
- The upper reservoir pressure, pressure drop across the specimen, flow pressure, flow rate, and air temperature entering the upper reservoir were recorded.

3.5.2 Specimen Performance

3.5.2.1 Microporous Composites - The seven microporous specimens described in Table II were tested in the screening test apparatus shown in Figure 38 with results shown in Figure 40 in the form of normalized pressure loss, $\sigma\Delta P_T$, versus actual mass flow rate of air per unit surface area. It may be noted that specimen MPC101 was tested both prior to and after sanding the surface to remove the resin coating. The performance lines shown were drawn through the available data points by visual inspection based on the general trends for the other test specimens. Results indicate that all specimens except MPC103, which is marginal at best, have much too high a pressure loss through the specimen at the required mass flow rate. Increasing the porosity to reduce the pressure loss would result in a reduction to the already marginal mechanical properties. Because of their high porosity and irregular pores, these microporous composites would be easily contaminated, but difficult to clean, because of their lengthy and tortuous flow paths. From these preliminary physical, mechanical, and flow property observations, microporous composites were eliminated from further detailed analysis.

3.5.2.2 Perforated Composites - Test results for 18 perforated composite test specimens, described in Table III, are shown in Figures 41 through 45 in the form of normalized pressure loss versus actual mass flow rate. All test data points are shown, and the performance lines are drawn through the data points by visual inspection. Figures 41 through 43 illustrate performance variations as a function of percent open areas at

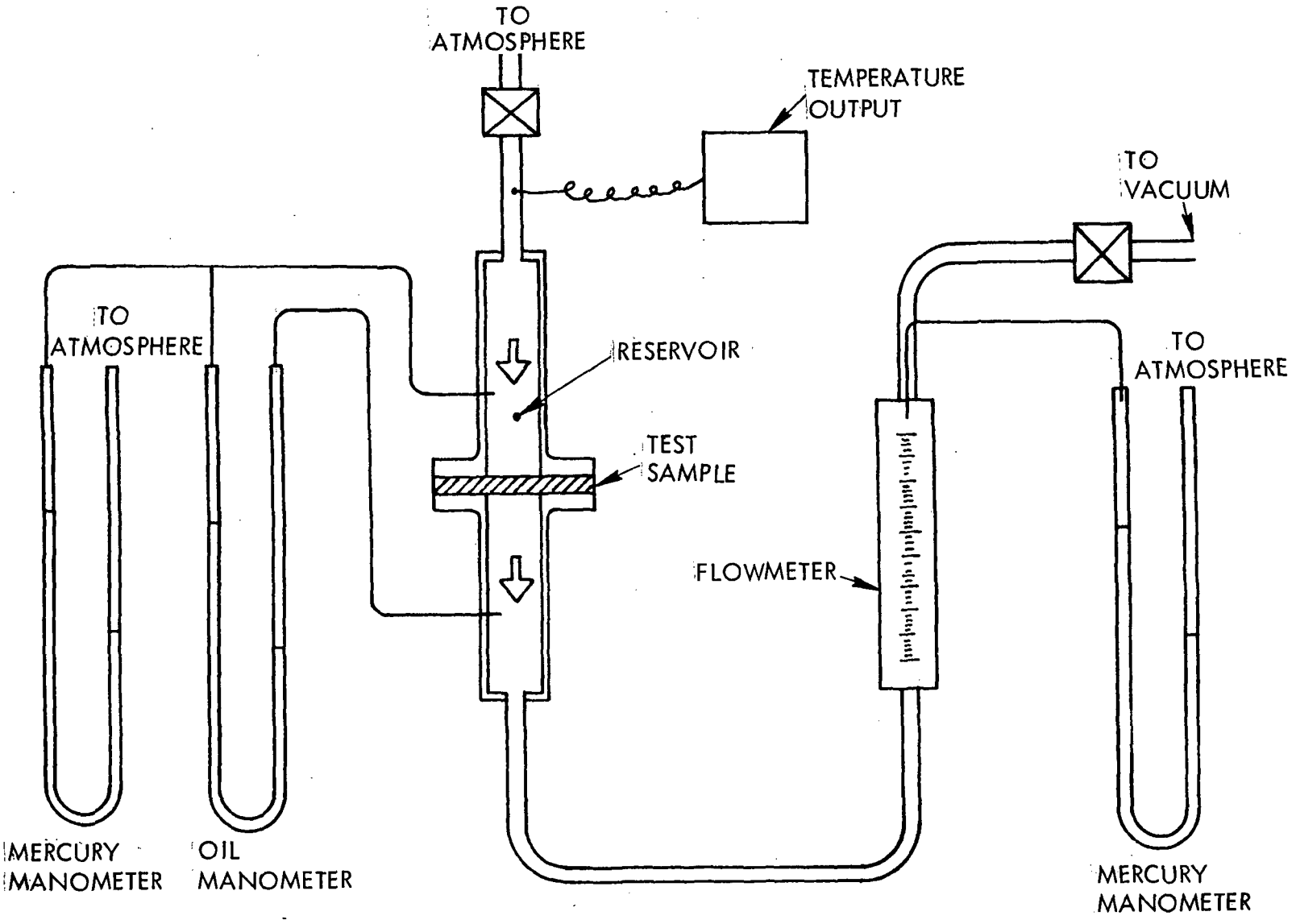

FIGURE 39. FINAL TEST APPARATUS

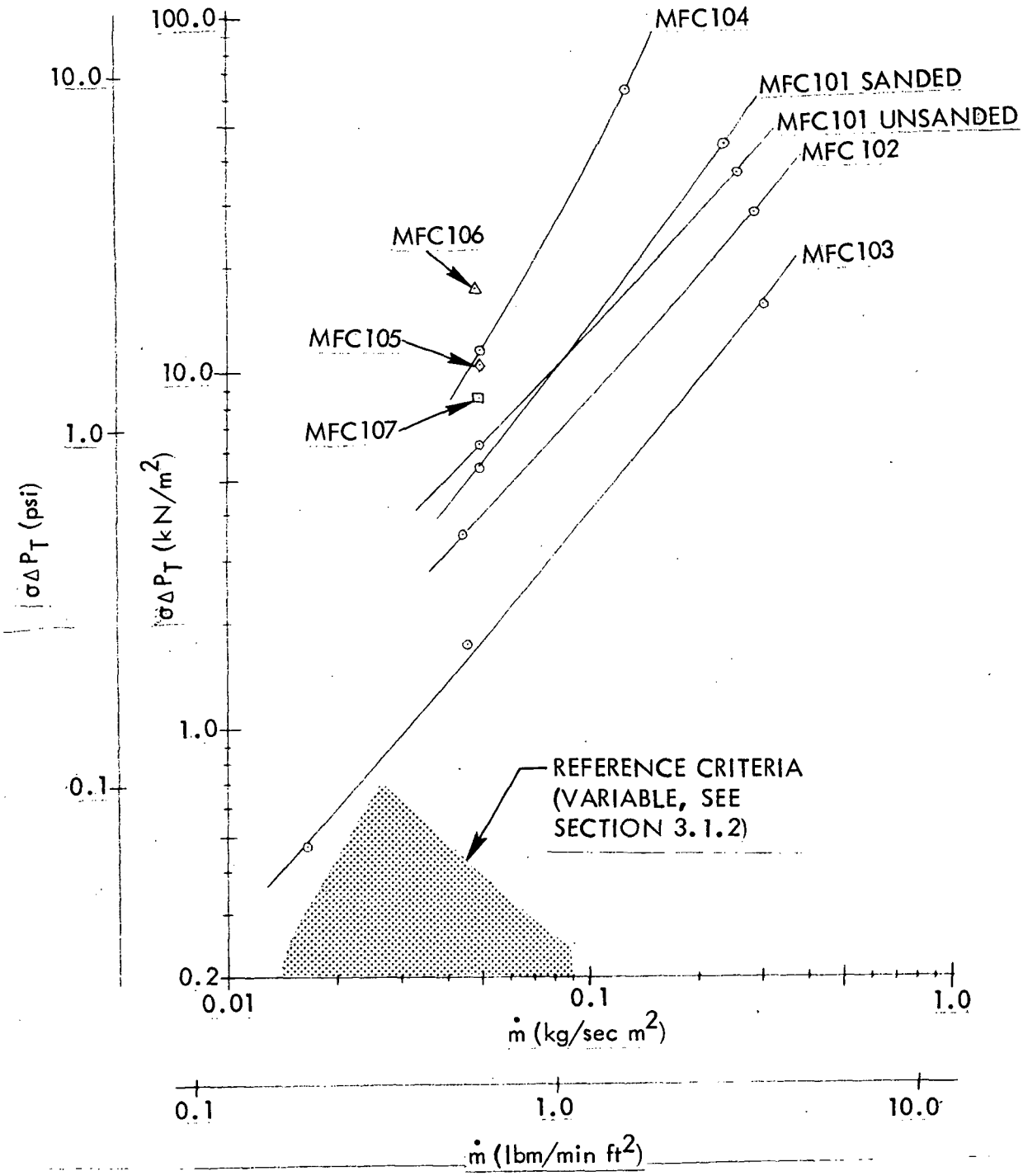

FIGURE 40. MICROPOROUS SPECIMENS

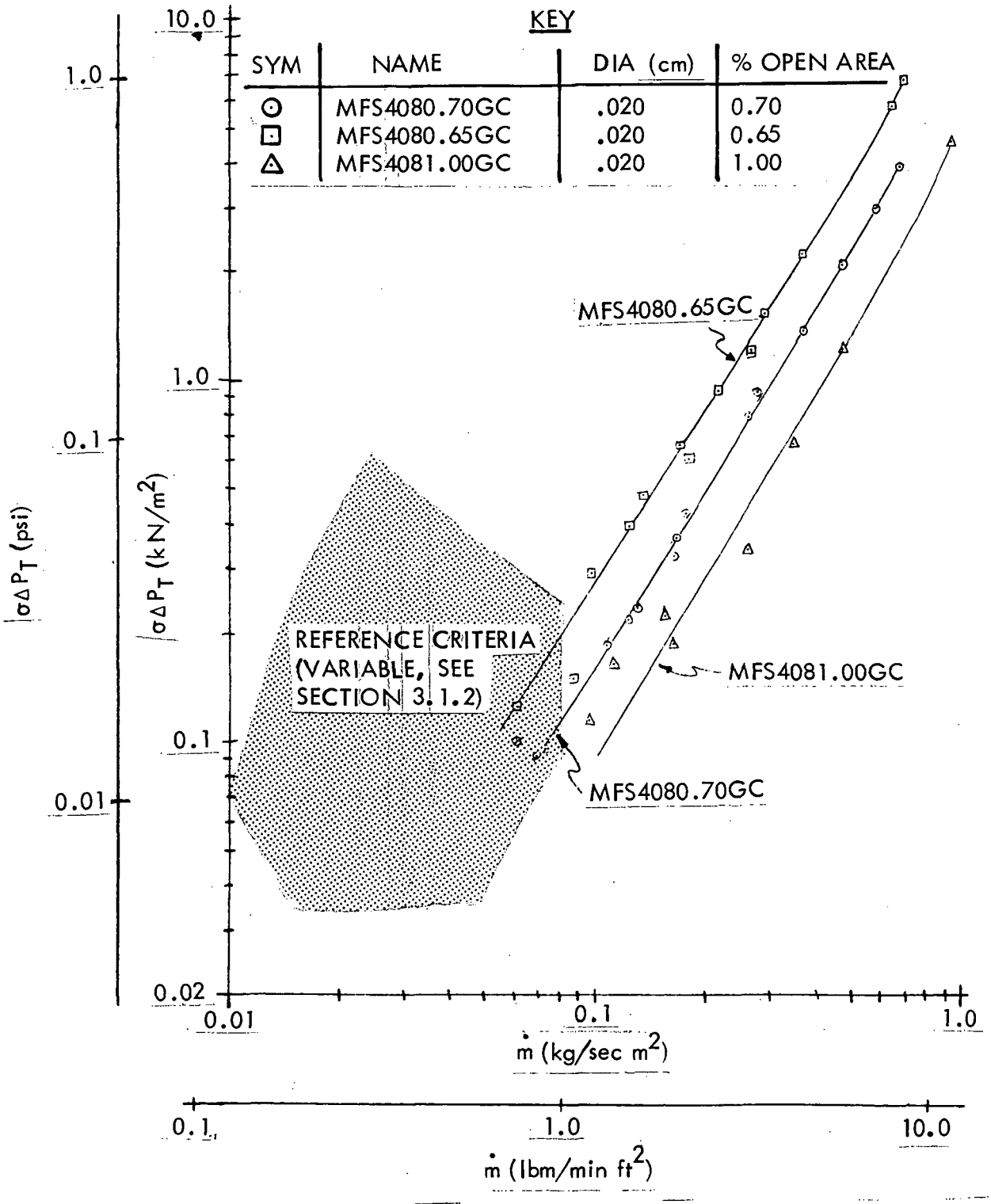

FIGURE 41. FLOW PERFORMANCE OF COMPOSITES PERFORATED WITH 0.020 cm DIAMETER MONOFILAMENT

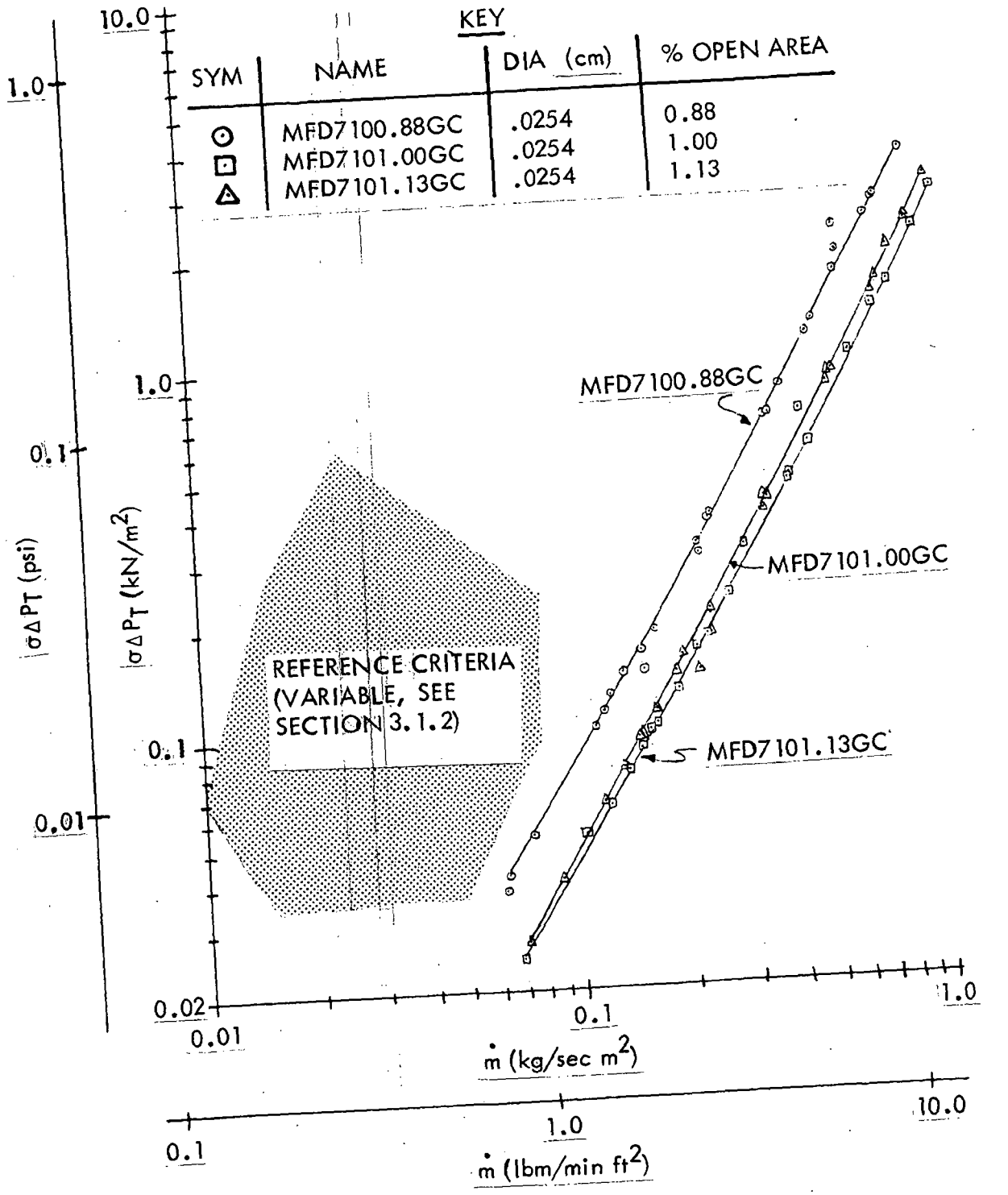

FIGURE 42. FLOW PERFORMANCE OF COMPOSITES PERFORATED WITH 0.025 cm DIAMETER MONOFILAMENT

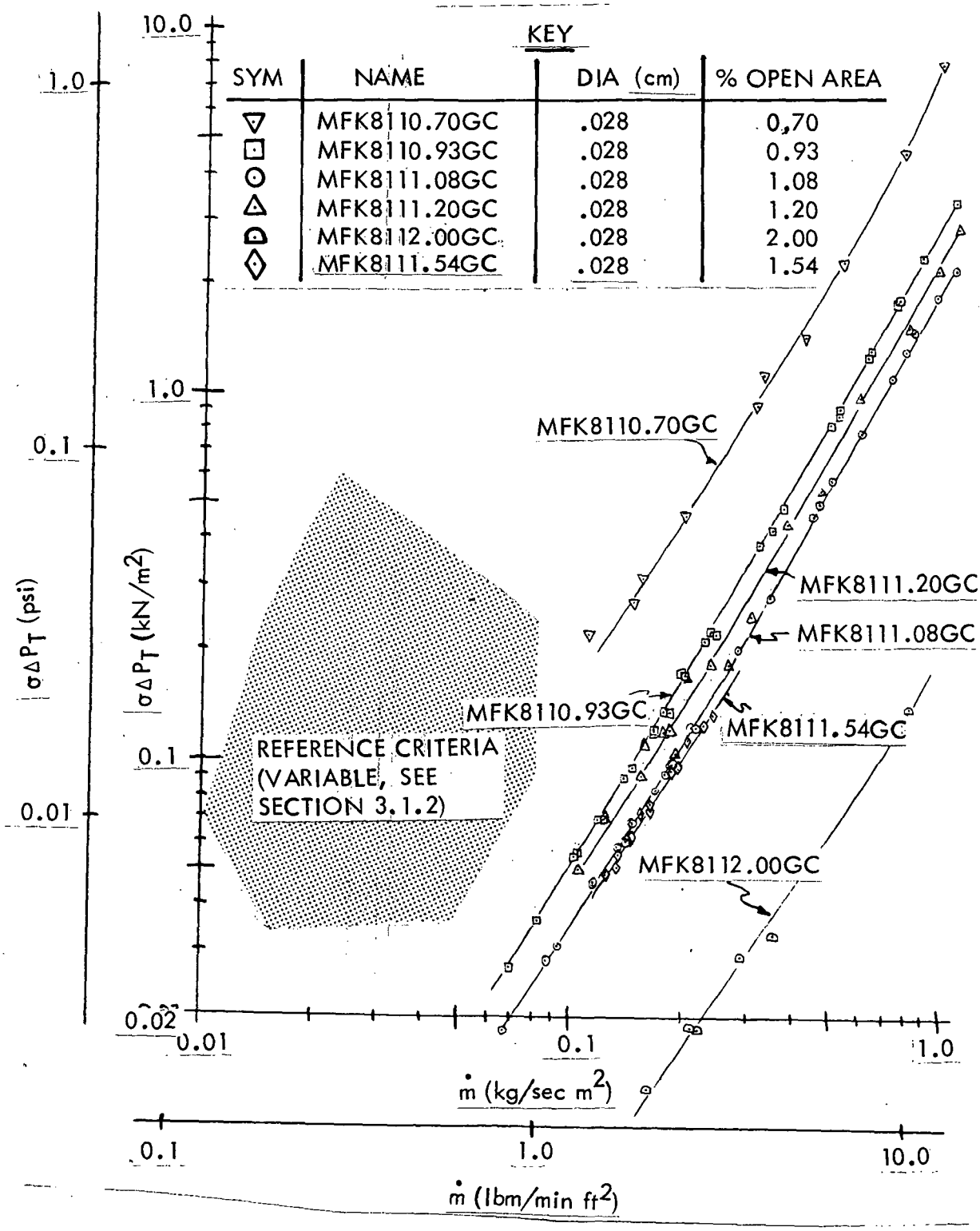

FIGURE 43. FLOW PERFORMANCE OF COMPOSITES PERFORATED WITH 0.028 cm DIAMETER MONOFILAMENT

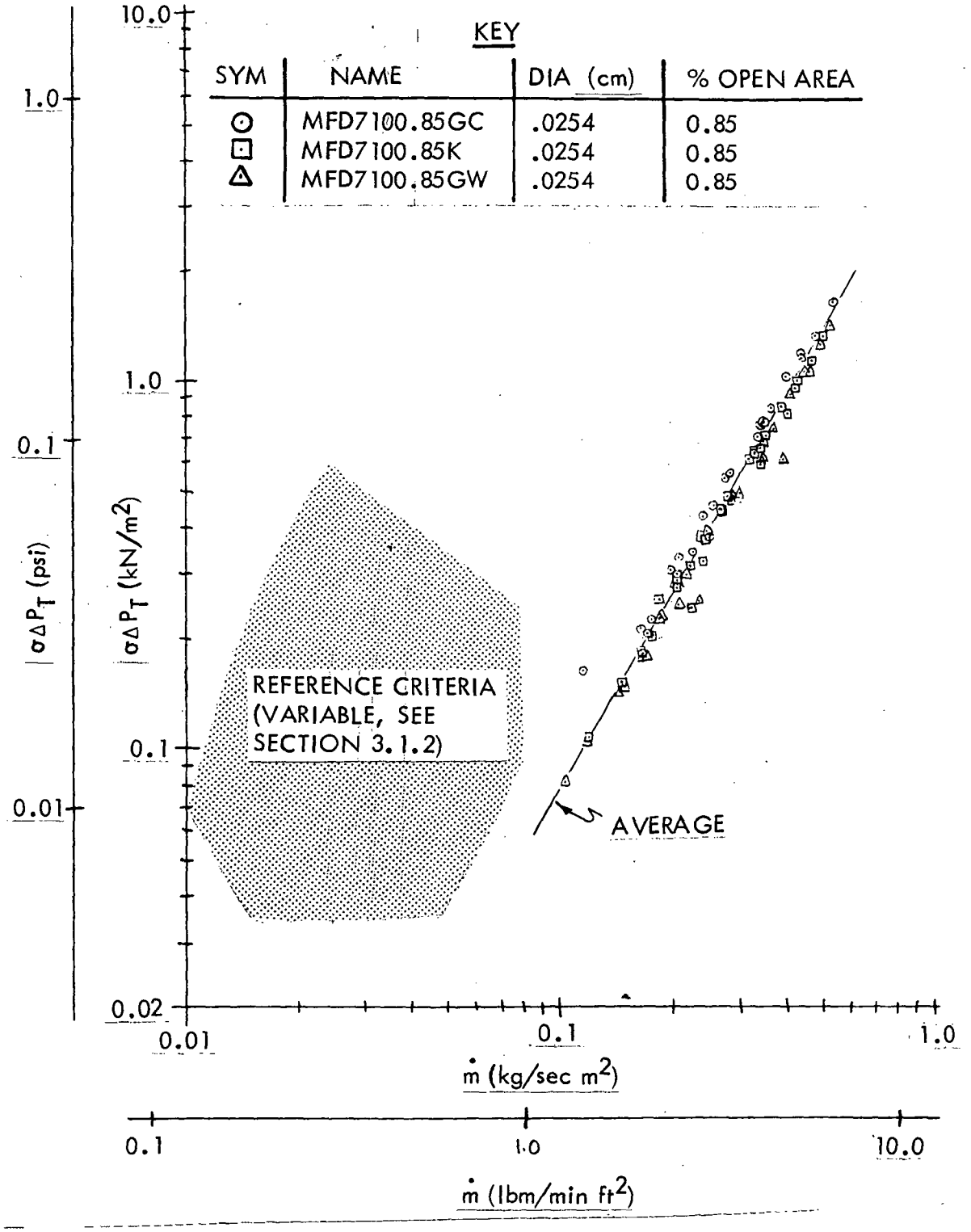

FIGURE 44. FLOW PERFORMANCE OF THREE COMPOSITES PERFORATED AT 0.85 PERCENT CALCULATED OPEN AREA

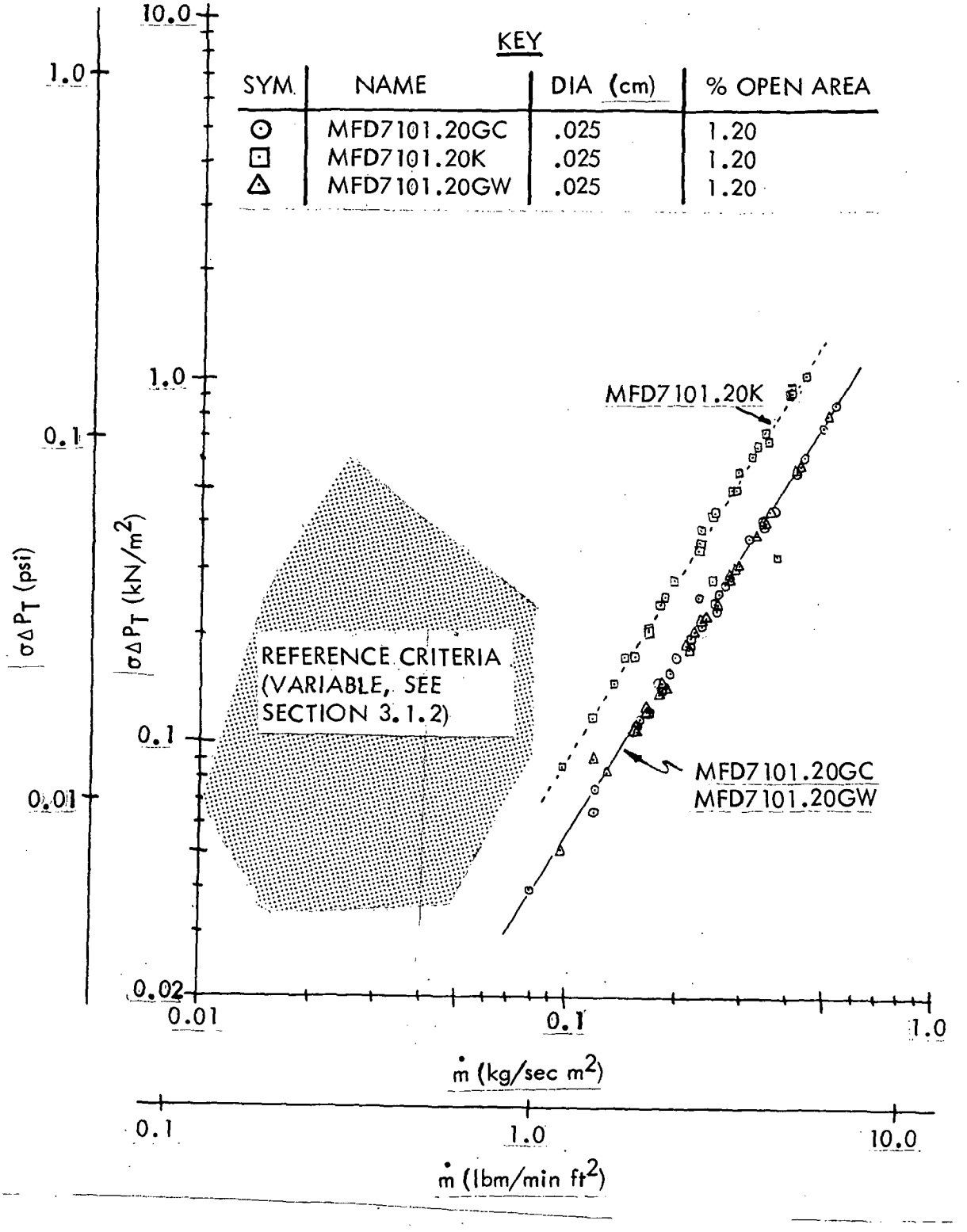

FIGURE 45. FLOW PERFORMANCE OF THREE COMPOSITES PERFORATED AT 1.20 PERCENT CALCULATED OPEN AREA

constant hole diameters. It was observed that the hole diameters produced by the fugitive fiber process are irregular, as discussed in subsection 3.4.2.2. Resin breakout between holes creates larger hole diameters and percent open areas than indicated by the fugitive fiber thread size. Therefore, it is noted that the percentage open areas listed on Figures 41 through 45 are calculated based on the fugitive fiber diameter and the number of stitches per unit area, and may vary considerably from the actual values. Tests of two configurations each of three fabric/epoxy laminates are shown in Figures 44 and 45. The uniformity of results shown in Figure 44 indicates, as expected, that the performance of these specimens is independent of the materials used in fabrication. Figure 45, on the other hand, indicates a variation in performance of MFD7101.20K from that indicated by MFD7101.20GC and MFD7101.20GW. Further investigation of this discrepancy reveals that the performance line of MFD7101.20K is the same as the performance line of MFD7100.85GC, MFD7100.85K, and MFD7100.85GW, shown in Figure 44. Subsequent visual investigation of MFD7101.20K indicated that it was not the same configuration as any of the three specimens shown in Figure 44. Because of these observations, MFD7101.20K was retested and verified the initial results. Further examination of this specimen showed incomplete dissolution of the fugitive fiber, accounting for the lower effective percent open area. Because of the excellent data correlation for all three composites shown in Figure 44 and the excellent agreement of the data from specimens MFD7101.20GC and MFD7101.20GW shown in Figure 45, it is concluded that the material type has no effect on the flow performance.

Comparison between the reference design criteria for the LFC-200-S aircraft (Reference 2) discussed in subsection 3.1.2 and the fugitive-fiber test results of Figures 41 through 45 shows that MFS4080.65GC, MFS4080.70GC, and MFK8110.70GC can be used for some wing surfaces if the total percent of porous surface area on the wing is reduced by decreasing surface porous strip width or increasing strip spacing. All other fugitive-fiber specimens tested can be used for any wing surface by again reducing the total percent of porous wing area in the same manner as previously described.

3.5.2.3 Perforated Metal - Test results for the nine electron-beam-perforated aluminum test specimens described in Table IV are shown in Figures 46 through 48 in the form of normalized pressure loss versus actual mass flow rate per unit surface area. Again, all the test data points are shown and the performance lines are drawn through the data points by visual inspection. Figures 46 and 47 show the performance curves for all EB specimens tested. Figure 48 investigates the relationship between diameter variation at a constant percent open area. Note from Figure 48 that the smaller diameter perforations at the same porosity have a different slope and larger pressure loss at the same mass flow rate than do the larger diameters as, for example, in the case of performance curves EB2 and EB8. The explanation is believed to be in the greater overall flow shear area when the open area is provided by small holes rather than large holes. This would indicate that the greater pressure loss could be due in part to increased viscous pressure losses as a result of the increased shear surface of EB2 over EB8. Additionally, to investigate whether the analytical methodology can account for large changes in temperature, EB2, EB5, and EB8 were tested and results compared at both 294°K (70°F) and 269°K (25°F) with no apparent discrepancies.

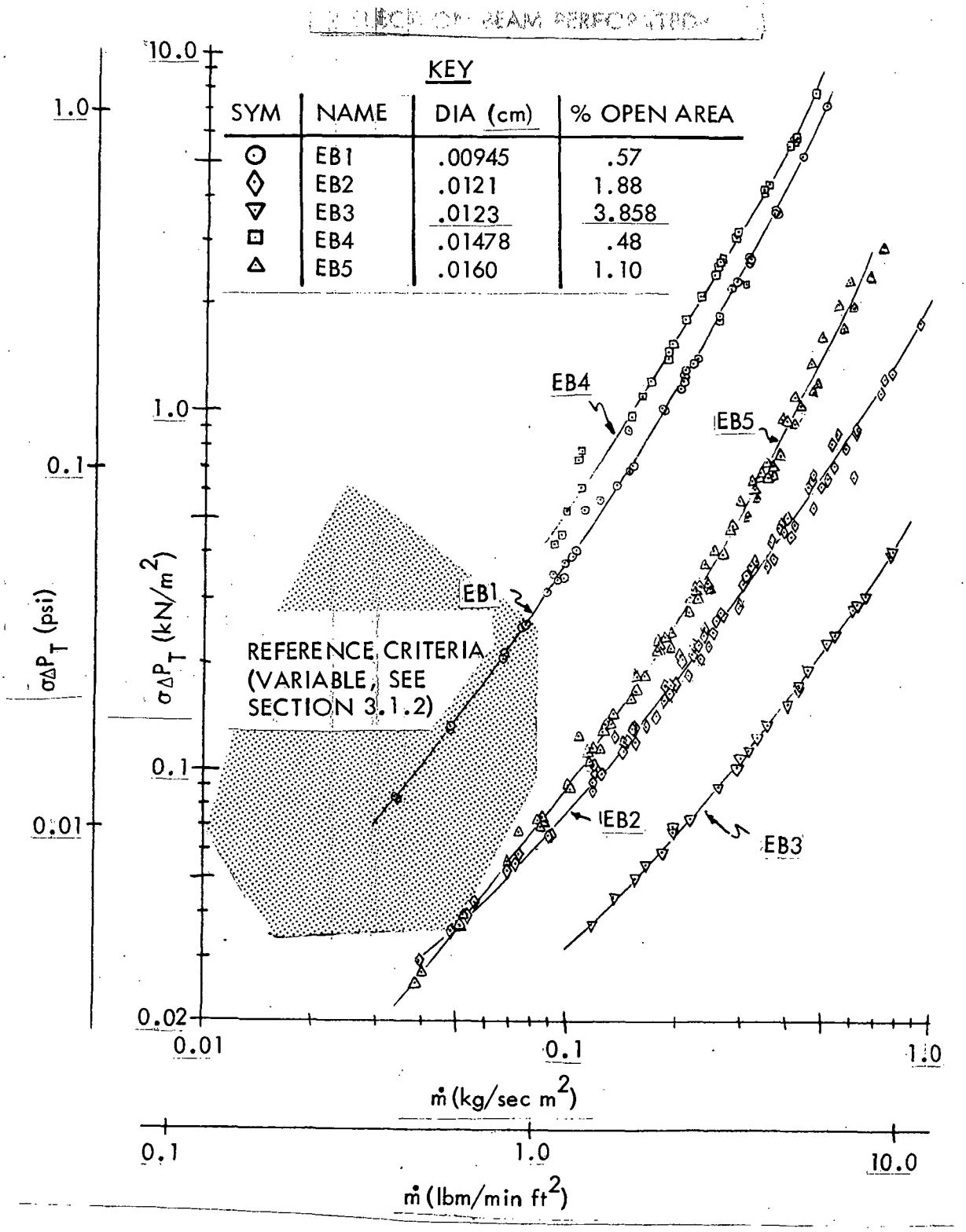

FIGURE 46. FIVE EB PERFORATED PANELS WITH VARYING PERCENT OPEN AREAS

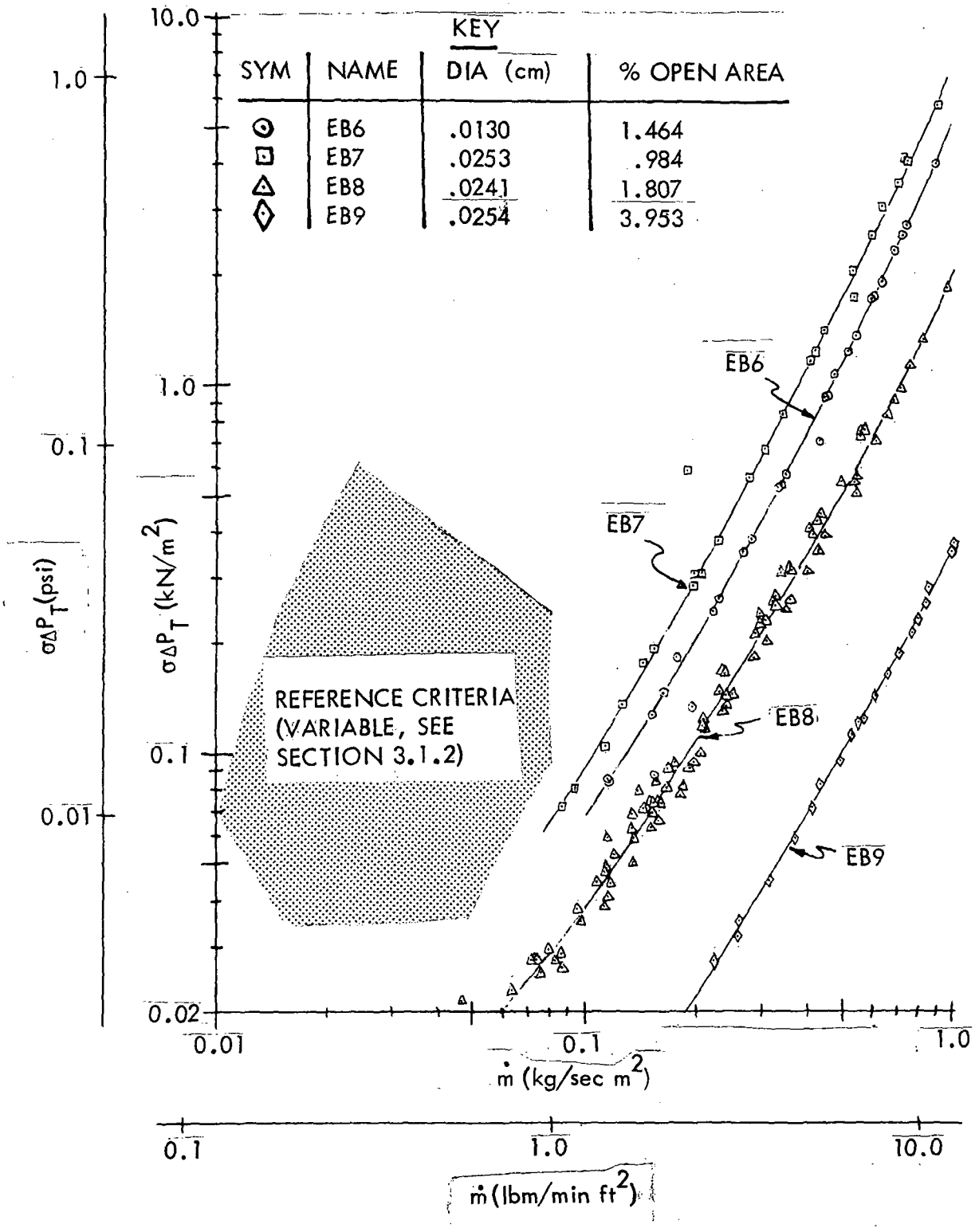

FIGURE 47. FOUR EB PERFORATED PANELS WITH VARYING PERCENT OPEN AREAS

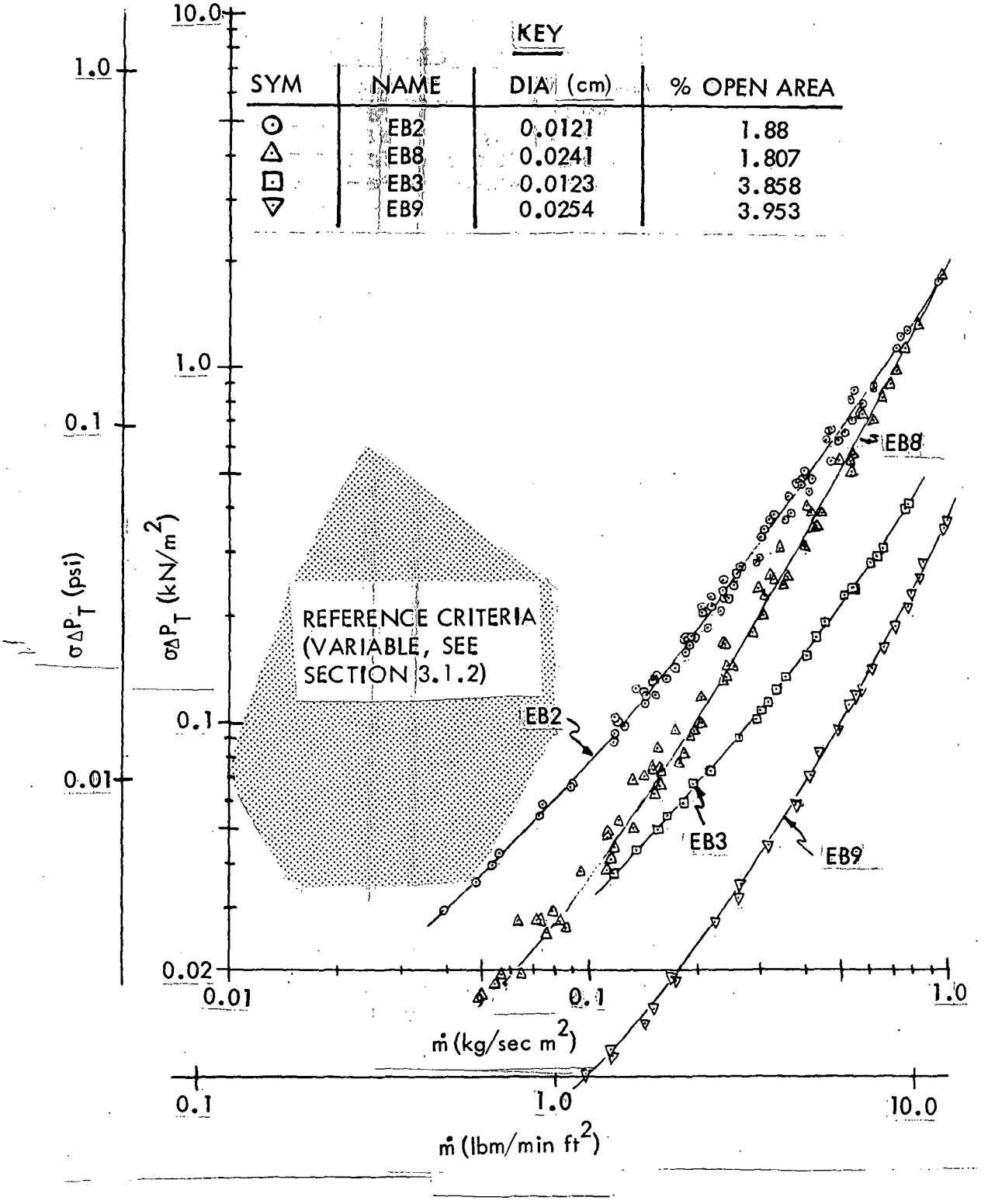

FIGURE 48. FOUR EB PERFORATED PANELS FOR EVALUATION OF DIAMETER VARIATION AT CONSTANT PERCENT OPEN AREAS

Comparison between the design criteria for the LFC-200-S aircraft (Reference 2) discussed in subsection 3.1.2 and the electron-beam-perforated specimen flow test results of Figures 46 and 47 indicate that EB1 and EB4 can be used for some wing surfaces if the total percent of porous surface area on the wing is reduced by decreasing surface perforated strip widths or increasing strip spacing. All other EB-perforated specimens tested can be used for all wing surfaces by reducing the total percent of porous wing area in the same manner as previously described.

3.5.2.4 Slots - The nine slotted specimens described in Table V were tested in the test apparatus shown in Figure 39 with results shown in Figures 49 and 50 in the form of normalized pressure loss versus actual mass flow rate of air per unit length of slot. All data points are shown, and performance lines are drawn through the data points by visual inspection. Two effects were investigated in these tests. Figure 49 presents the effect of varying slot width in a constant material thickness, while Figure 50 displays the variation in performance for constant slot widths in varying sheet thicknesses. Figure 49 indicates logically an increase in pressure loss as the slot width decreases. The trend of Figure 50 is partially obscured by some variation in slot width between samples. However, a comparison of S5 and S6, which have equal slot widths, with S7 and S9, which have approximately equal slot widths, indicates a slight trend of increasing pressure loss with increasing material thickness as would be expected. An overall comparison of the two figures shows that by far the most influential factor in the variation of performance curves is the slot width, while the material thickness appears to have less effect on pressure loss.

Comparison between the design criteria for the LFC-200-S aircraft (Reference 2) discussed in subsection 3.1.3 and the slotted specimen test results shown in Figures 49 and 50 indicates that all specimens except S4 could be used with some of the wing surfaces by varying the slot spacing as discussed in subsection 3.1.3. On the other hand, S4 could be used for any wing surface by changing the slot spacing as described in subsection 3.1.3.

3.5.3 Contamination Studies

Three of the EB-perforated aluminum panels were exposed to contamination media to determine the effects of that exposure on the flow characteristics and performance, and to evaluate the effectiveness of cleaning procedures.

Panel EB2 was exposed to engine exhaust gases for one week by placing the panel in the Production Flight Test C-130 engine run-up area, duplicating the effect on an aircraft exposed to exhaust from nearby aircraft. The panel was backflushed with air and flow-tested. It was cleaned by vapor degreasing and again flow-tested. These test results are plotted in Figure 51 along with precontamination test results. Examination indicates that for a given mass flow rate, the engine run-up contamination resulted in an increased pressure loss of approximately nine percent. The cleaning process removed the contamination residue from the panel well enough to restore its original performance.

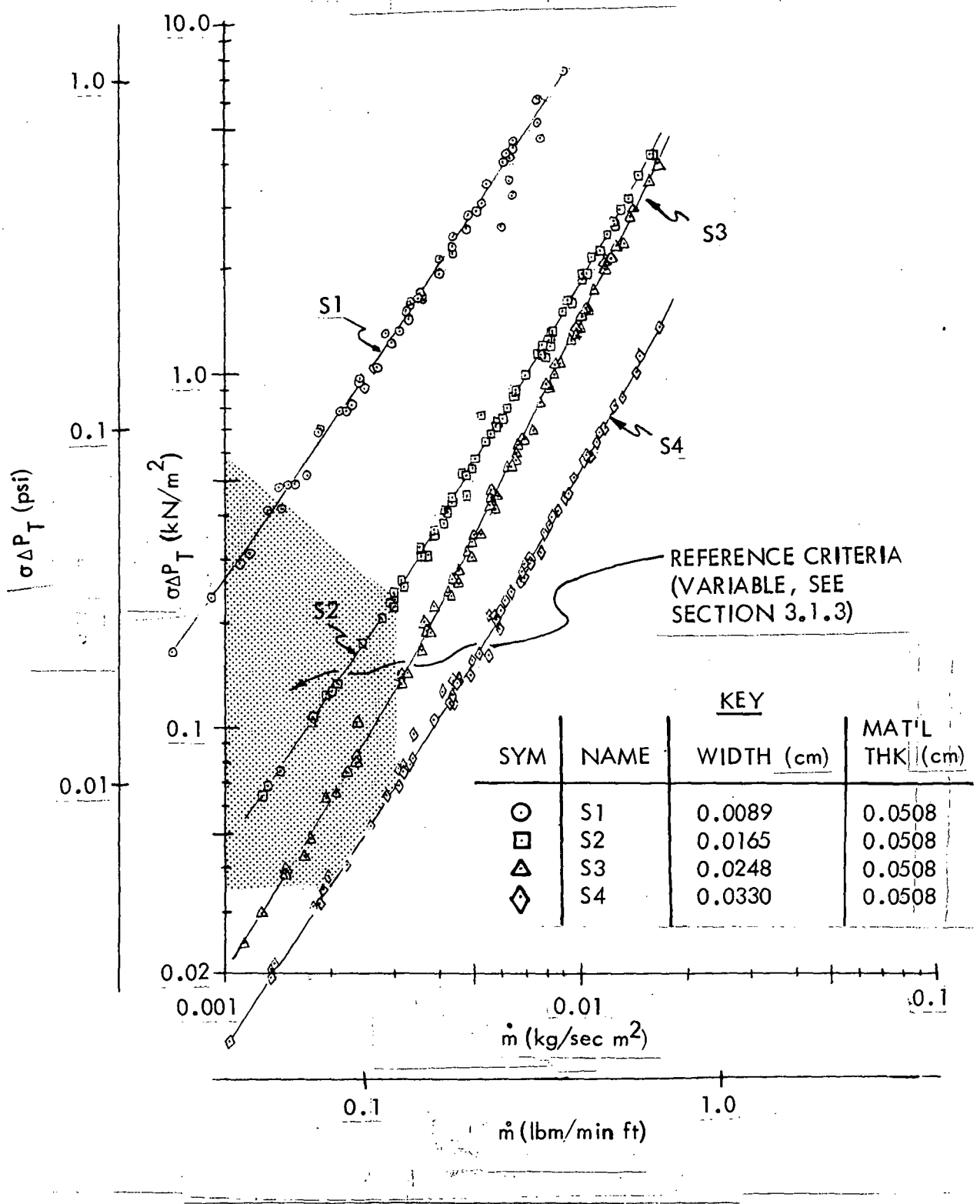

FIGURE 49. FLOW PERFORMANCE OF SLOTS WITH VARYING SLOT WIDTH

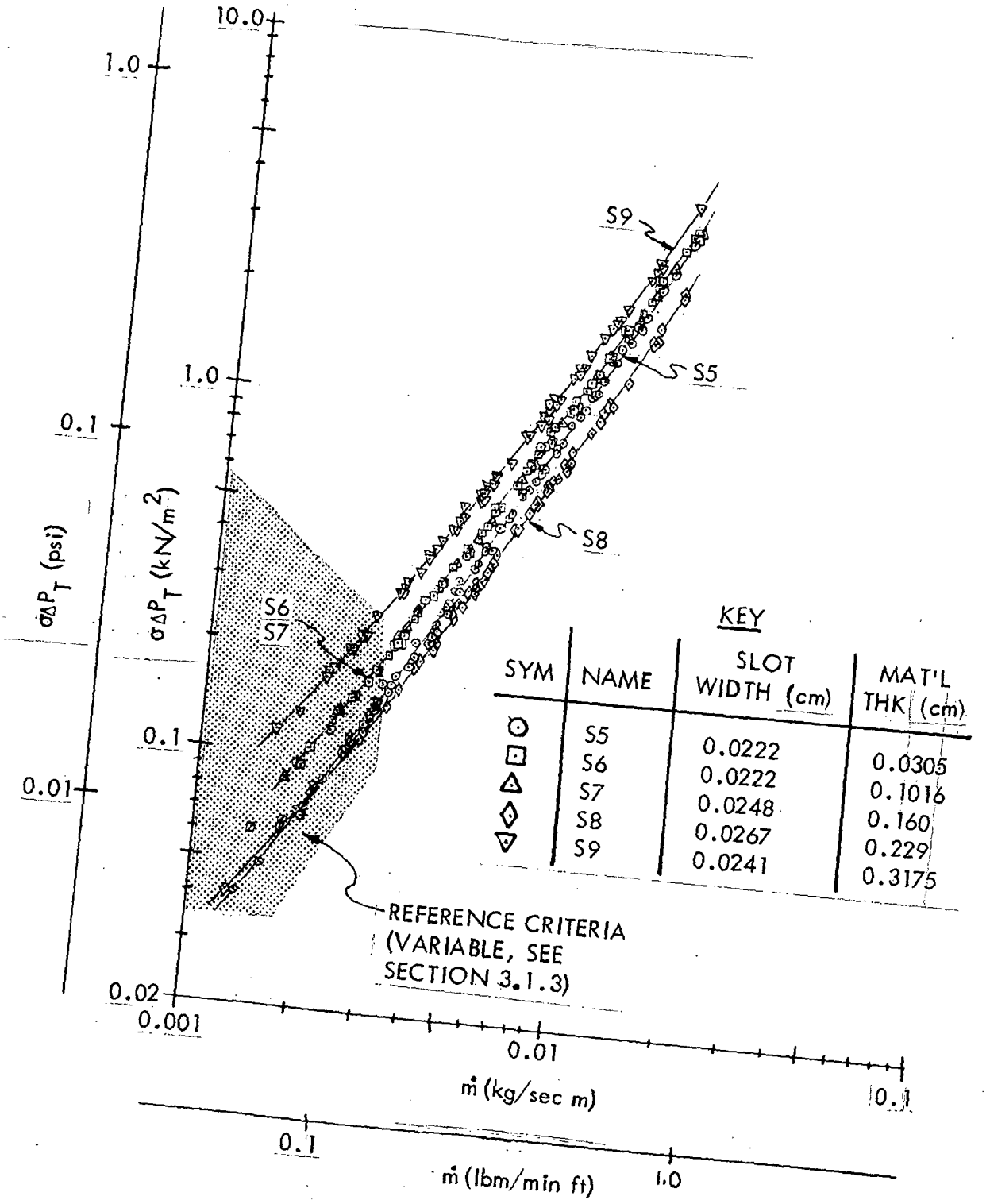

FIGURE 50. FLOW PERFORMANCE OF SLOTS WITH VARYING MATERIAL THICKNESS

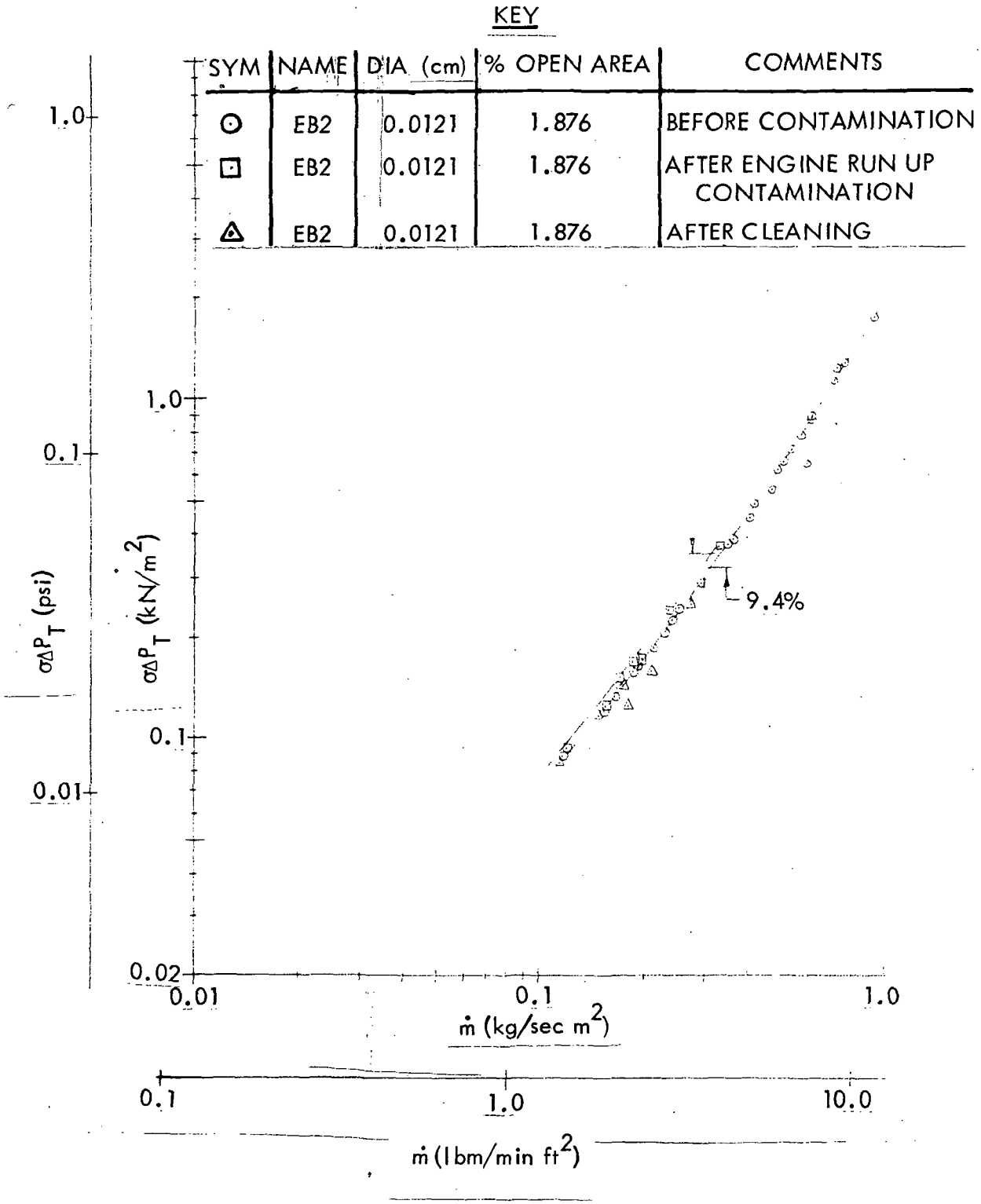

FIGURE 51. FLOW PERFORMANCE OF EB2 CONTAMINATED BY EXPOSURE TO ENGINE EXHAUST FOLLOWED BY CLEANING

Panel EB7 was first exposed to a dusty environment, which would be representative of an airplane on the ground in dry weather, by wiping finely divided dirt over the specimen and into the holes. It was then backflushed with air and flow-tested. Next, the same panel was flooded with low-viscosity peanut oil, excess oil blown off with air, redusted in the same manner as before, backflushed with air, and again flow-tested. This second condition is considered representative of contamination from common maintenance operation. Finally, EB7 was cleaned by vapor degreasing and again flow-tested. All the EB7 panel precontamination and contamination test results are plotted in Figure 52. The results of the contamination indicates that, at the same mass flow rate, the dust contamination increased pressure losses by about 10 percent, and the dust and oil contamination increased pressure losses to about 21 percent over the precontamination condition. Again, the cleaning method appears to have successfully removed the contamination residue.

Panel EB8 was exposed to dust in the same manner as described for panel EB7, and exposed to 98% relative humidity, followed by heating at 322°K (120°F) until the moisture dried, then backflushed with air, and flow-tested. This condition represented an airplane on the ground during alternately wet and dry hot weather. After flow testing, panel EB8 was cleaned by vapor degreasing and again flow-tested. Figure 53 contains a plot of the precontamination, contaminated, and cleaned test results. These results indicate a 28 percent increase in pressure loss at the same mass flow rate as a result of the dust, moisture, and heat exposure. However, the cleaning process was only partially successful, since the cleaning resulted in only a 12 percent decrease in pressure loss from the contaminated condition.

When the results of Figures 51 through 53 are compared with the design criteria for the LFC-200-S aircraft (Reference 2) discussed in subsection 3.1.2, it is indicated that all specimens could be used for any wing surface after minor modification to increase the porous/perforated suction surface spacing on the wing surface.

3.6 FLOW TEST ANALYSIS

3.6.1 Theory

The purpose of the analytical effort is to develop a method of predicting pressure loss through a test specimen as a function of suction flow rate with known ambient conditions and flow path dimensions. Although the normalized pressure loss versus actual mass flow rate graphs eliminate the altitude pressure effects, it does not account for the effects of hole diameter or slot width, material thickness, and percent open area as was presented in Section 3.5. Therefore, further investigation was carried out. The suction requirements and the ratio of length to diameter or length to slot width indicated a laminar flow analysis should be used. Due to the short length of the flow path through the surface material, determined by the thickness of the slotted or perforated material, a hydrodynamic entry length analysis was investigated to account for the entry length losses, which are greater than the fully developed flow losses. Reference 5 presents a method of obtaining a solution to the pressure loss in the hydrodynamic transition length of a straight tube with a round inlet by a linearizing approximation to the Navier-Stokes equation. Basically, the pressure loss relationship can be represented by:

KEY

SYM	NAME	DIA (cm)	% OPEN AREA	COMMENTS
⊙	EB7	0.0253	0.984	BEFORE CONTAMINATION
⊡	EB7	0.0253	0.984	AFTER DUST CONTAMINATION
◇	EB7	0.0253	0.984	AFTER DUST & OIL CONTAMINATION
△	EB7	0.0253	0.984	AFTER CLEANING

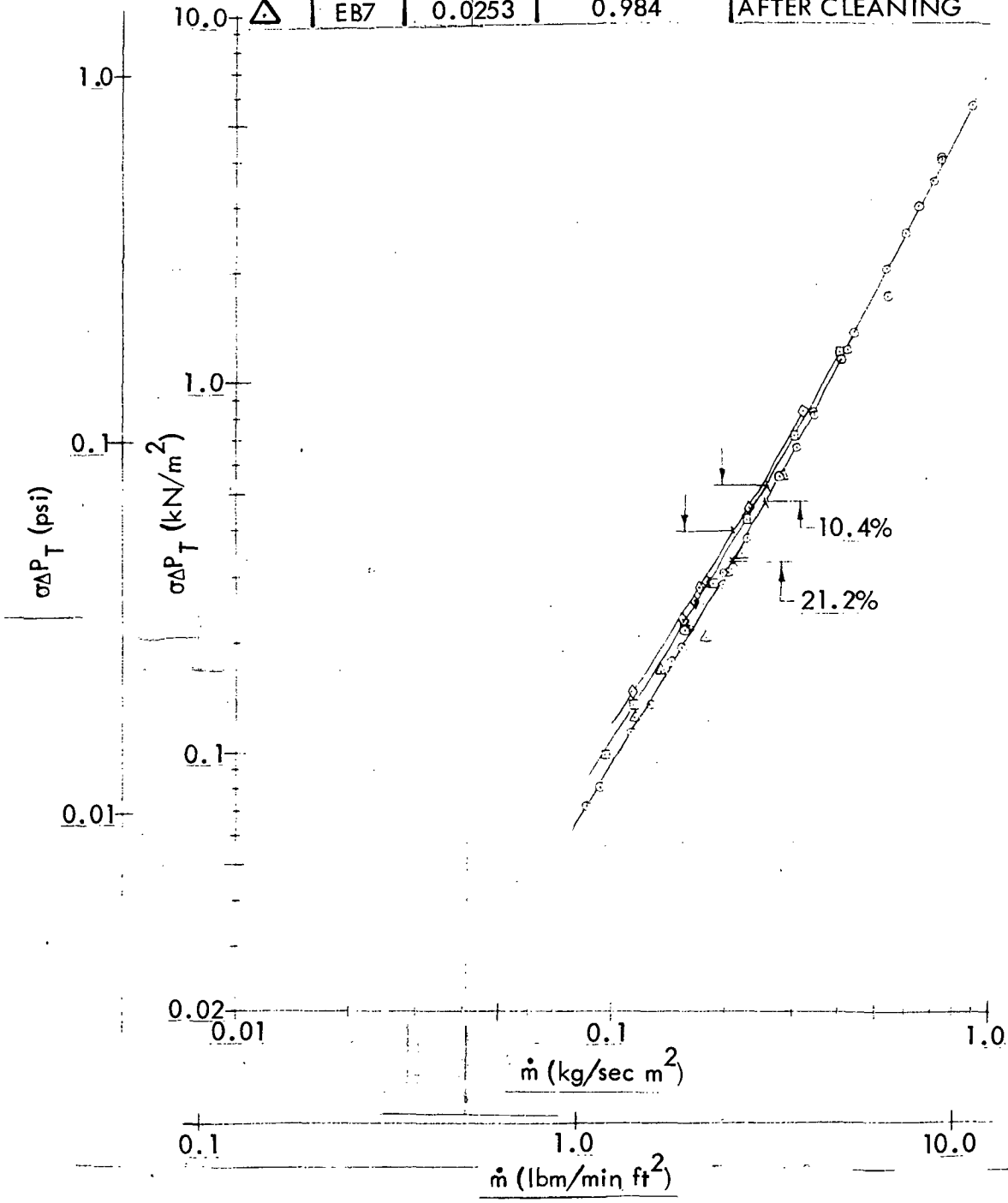

FIGURE 52. FLOW PERFORMANCE OF EB7 CONTAMINATED WITH DUST, DUST AND OIL, FOLLOWED BY CLEANING

KEY

SYM	NAME	DIA (cm)	% OPEN AREA	COMMENTS
⊙	EB8	0.0241	1.807	BEFORE CONTAMINATION
⊡	EB8	0.0241	1.807	AFTER DUST & MOISTURE CONTAMINATION
△	EB8	0.0241	1.807	AFTER CLEANING

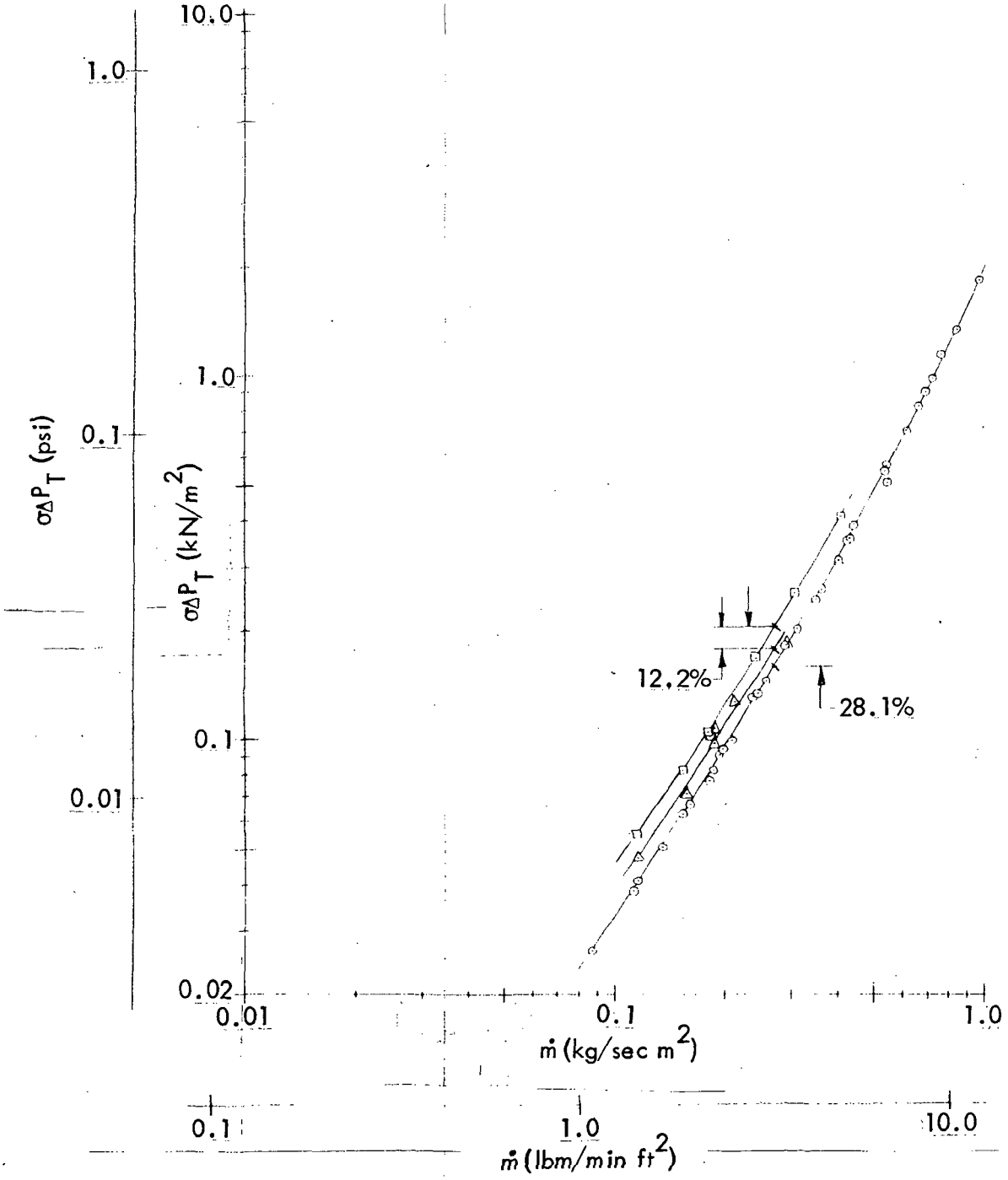

FIGURE 53. FLOW PERFORMANCE OF EB8 CONTAMINATED WITH DUST AND MOISTURE FOLLOWED BY CLEANING

$$\Delta P = f \frac{\rho V^2}{2gc} \quad \text{and} \quad f = F(\beta) \tag{1}$$

where $\beta = \frac{4\Delta X}{D Re_D}$ for tubes, $\beta = \frac{\Delta X}{W Re_W}$ for slots, and f is an analytical friction factor. This analytical relationship for β is obtained by comparison of the equivalent hydraulic radius for tubes and slots. The velocity term used is the average hole or slot velocity and the pressure drop (ΔP) is equal to the pressure in the still reservoir upstream of the entrance minus the pressure at a distance, X, downstream of the entrance.

3.6.2 Data Analysis

Prior to substituting the test data in Equation (1) and solving for friction factor and β, each of the three types of skin surface candidates was investigated for applicability to the entry length theory used. Although none of the skin surfaces duplicated the theoretical tube, they were analytically corrected, where possible, for their deficiencies. The observed deviations for the perforated composites, perforated metal, and slotted specimens are discussed below.

Perforated Composite Specimens

The hole diameters created by the fugitive-fiber process were unpredictable, with material breakout between holes creating much larger hole diameters and percent open areas than the nominal hole sizes indicated by the stitch thread size. Furthermore, due to the inherent nature of the stitching process in a soft material, severe nozzling and diffusing effects are apparent in the results. These problems are apparent in the photos in Figures 23 and 24. Because of these deficiencies and the inability to predict adequately and to account for these effects in the theoretical analysis, friction factor versus β curves could not be accurately constructed for the perforated composite specimens.

Perforated Metal Specimens

As discussed in subsection 3.4.2.3, the electron-beam-perforated specimens were subjected to extensive microscopic evaluation. It was discovered that the EB holes are not straight tubes but are tapered as shown in Figure 27. Because of flow direction, the taper acts as a diffuser with square corner inlets. Since the inlet and exit diameters are known, flow properties at both the inlet and exit can be calculated, and the average of both used in solving for friction factor and β. These results are plotted in Figure 54.

Slotted Specimens

Investigation of the slotted specimens indicates that slot width stays relatively constant through the material thickness. The inlet is square-cornered and, in general, the physical parameters are very well defined. Plots of friction factor versus β, where $\beta = \frac{f}{W Re_W}$, for slots with varying slot widths and slots with varying material thickness are shown in Figures 55 and 56, respectively.

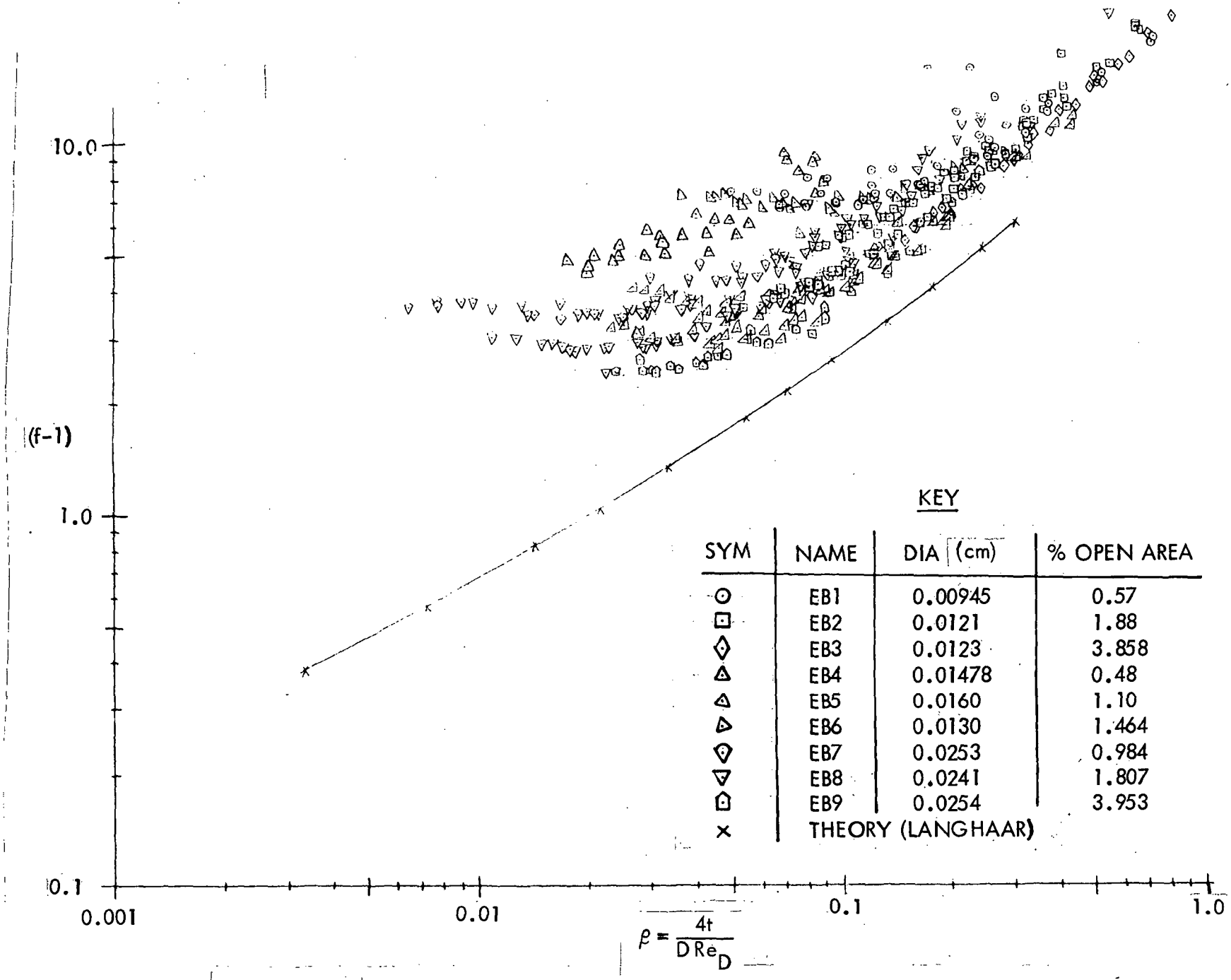

FIGURE 54. FRICTION FACTOR VERSUS β FOR EB PERFORATED SPECIMENS

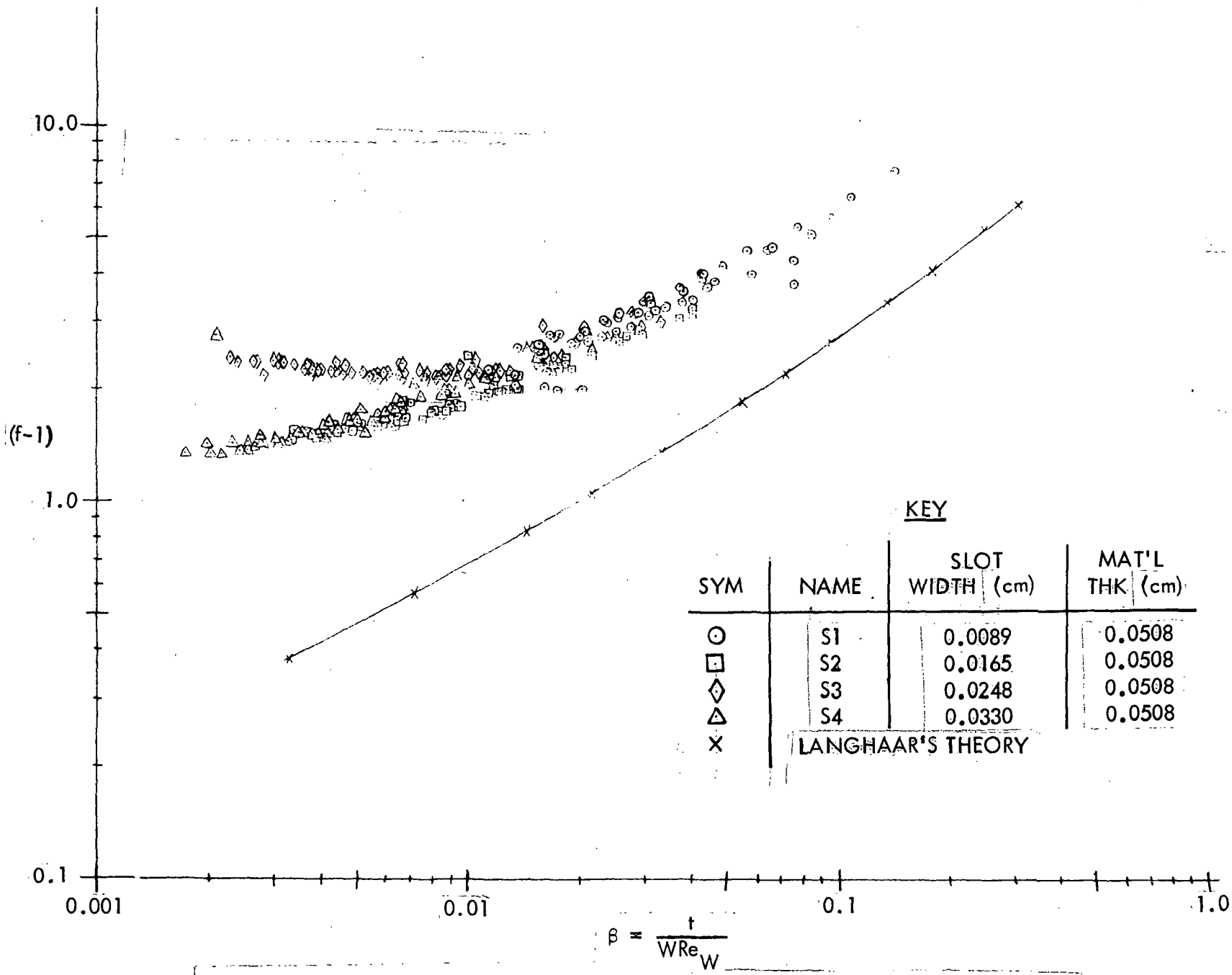

FIGURE 55. FRICTION FACTOR VERSUS β FOR SLOTS WITH VARYING SLOT WIDTH AND CONSTANT MATERIAL THICKNESS

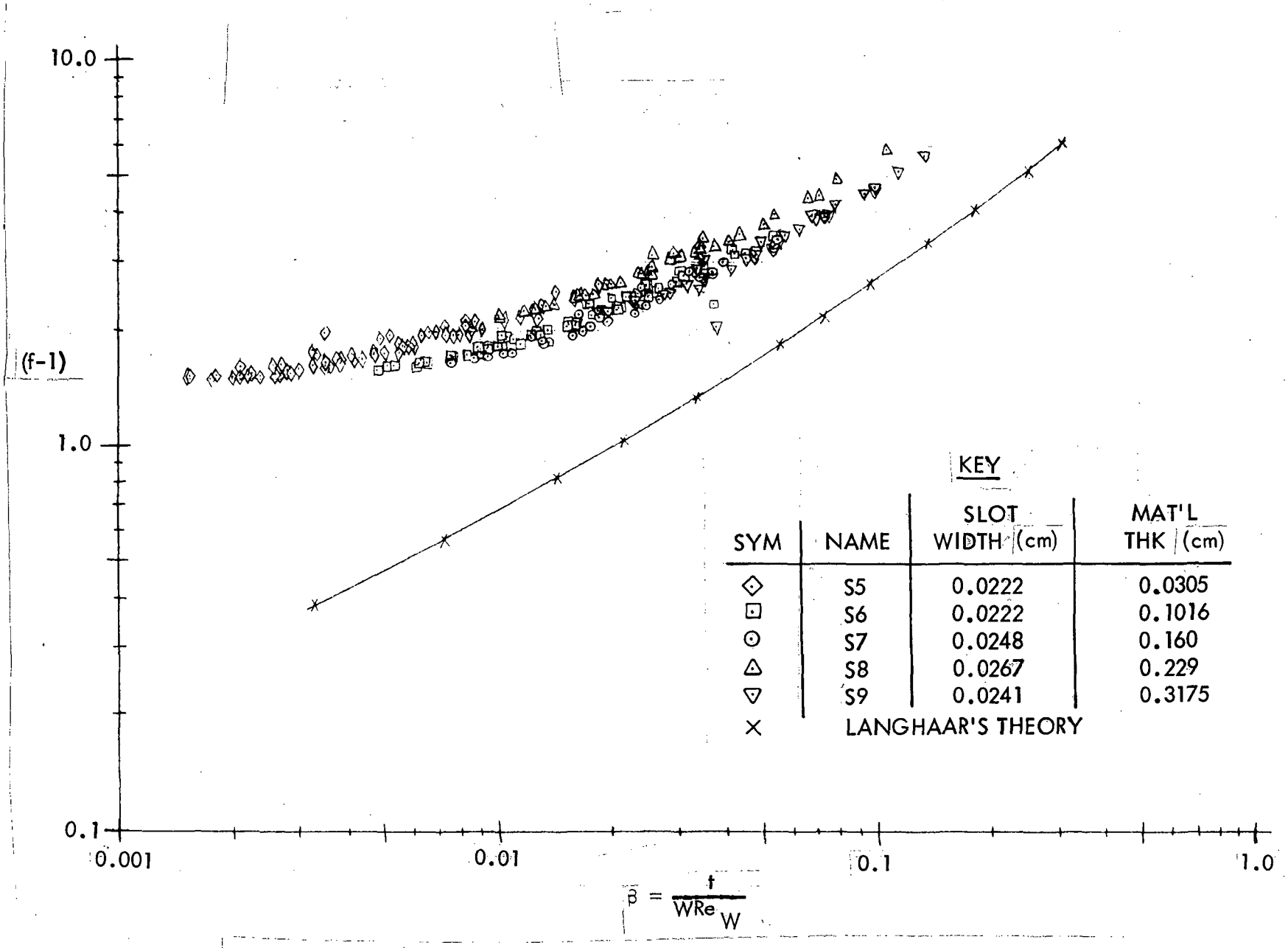

FIGURE 56. FRICTION FACTOR VERSUS β FOR SLOTS WITH VARYING SHEET THICKNESS AND CONSTANT SLOT WIDTH

Recall that $\sigma\Delta P_T$ versus actual mass flow rate curves reflect the performance of various suction surfaces. However, an accurate prediction of pressure loss/flow characteristics at a given altitude pressure condition cannot be made using a $\sigma\Delta P_T$ versus mass flow curve without first testing the specific specimen configuration for various pressure losses and flow rates to establish the performance curve itself. The consolidation of data presented in Figures 54 through 56 indicates that the parameters of the hole diameter or slot width, material thickness, and percent open area discussed earlier were accounted for in the analysis. This also gives the capability of generating a relationship between friction factor and β, and ultimately predicting pressure loss through a test specimen as a function of suction flow, altitude conditions, and physical properties of the specimen without the requirement for testing. This capability will prove to be a powerful tool. Although the experimental data give strong results, as summarized in Figure 57, the results indicate a higher pressure loss than the theoretical values from Reference 5, shown on Figures 54 through 57. Recall that the theoretical line was generated for a straight tube with a round inlet. The results of the electron beam perforations shown in Figure 54 were for neither a straight tube nor a rounded inlet, and the results of the slotted studies shown in Figures 55 and 56 were for square-cornered inlets. Therefore, a large portion of the discrepancy could be accounted for in the increased entrance losses incurred from the sharp inlet. Another possible factor influencing the higher friction factors could be the result of inexact diameter or slot width measurement. Examination of the significant basic dimensions that appear in evaluation of Equation (1) indicates that, among other parameters, the friction factor is proportional to the perforated hole diameter to the 4th power or the slot width to the 2nd power. However, β is independent of the perforated hole diameter and is an inverse function of the slot width. The effect of this variation can be amplified if the electron beam specimens are considered. If the maximum error in measuring the hole diameters of all EB specimens tested is ± 0.00127 cm (± 0.0005 in.), a variation of hole diameter from 4.5 to 13.3 percent is obtained which leads to a friction factor, and ultimately pressure loss, variation of from 19.3 to 64.8 percent.

As discussed earlier, the data consolidation summarized in Figure 57 gives the capability of generating a relationship between friction factor, which would ultimately be used to predict the pressure loss through the skin surface, and β. A hyperbolic equation of the form:

$$f = 27 \sqrt{\beta^2 + (2)\left(\frac{2}{27}\right)} + 2 \qquad (2)$$

where again β is defined as

$$\beta = \frac{4t}{D\,Re_D} \quad \text{or} \quad \beta = \frac{t}{W\,Re_W}$$

can be used to approximate a majority of the experimental data. It should be noted at this point that the EB data and the slotted data in Figures 54 through 56 tend to "flatten out" as both friction factor and β decrease. Each EB specimen seems to start its deviation from an asymptotic line at a different point which appears to be a function of the ratio of material thickness to hole diameter or slot width (t/D or t/W). Therefore, the relationship expressed in Equation (1) may vary from the experimental data as β falls below a critical value. However, for the range of flows tested, the effects of this

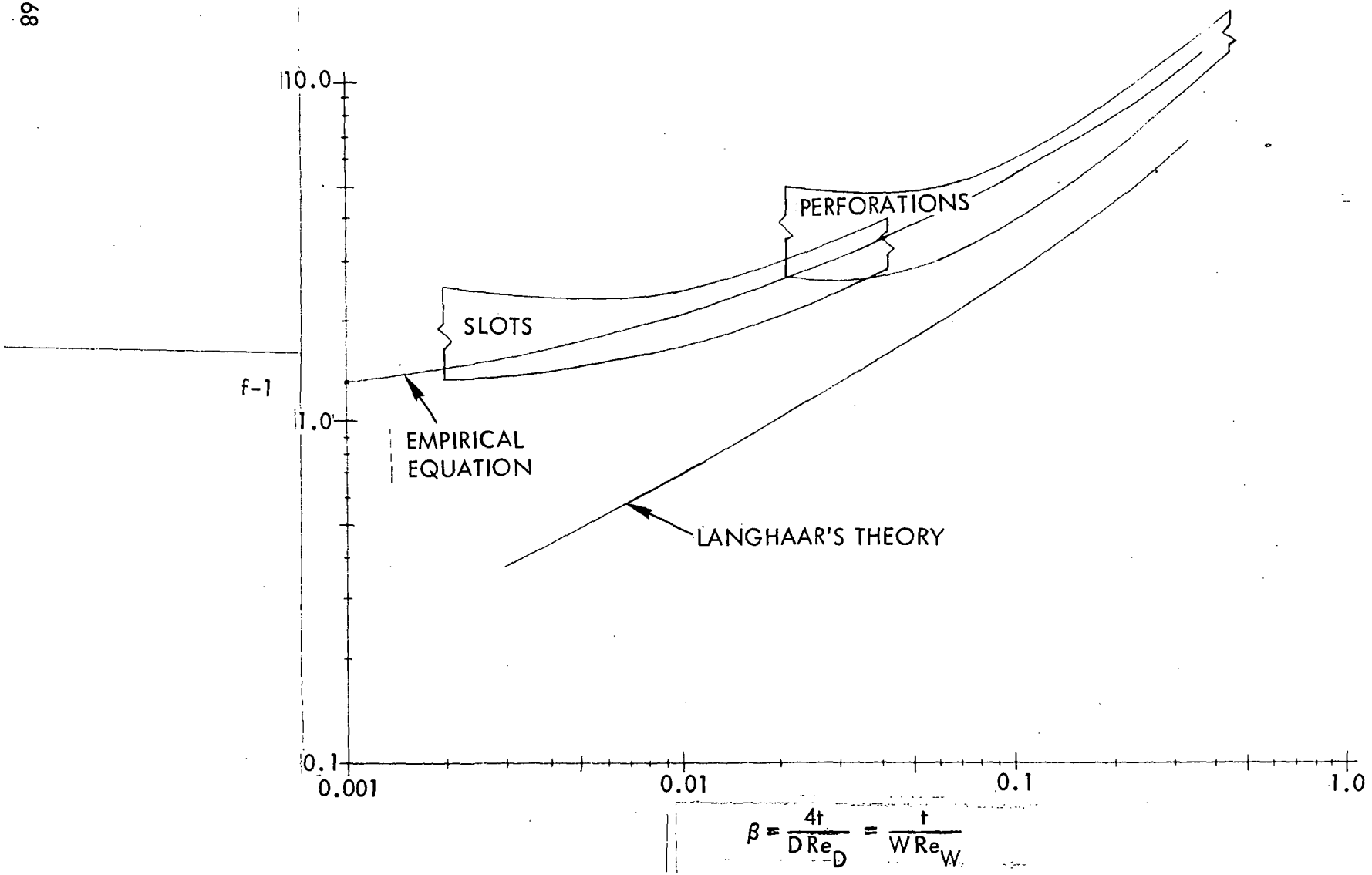

FIGURE 57. SUMMARY OF CALCULATED FRICTION FACTOR RESULTS

variation do not appear too severe. Further detailed analysis in this range is needed to determine accurately the cause and effect of this phenomenon, and provide methods for predicting the critical value of β and the characteristics of friction factor below this value.

4.0 TASK II - MECHANICAL PROPERTY MATERIAL

4.1 PANEL FABRICATION

Four 0.3 by 0.3 m (1 ft by 1 ft) perforated composite panels were fabricated and delivered to NASA for mechanical property testing. These four panels were perforated by the fugitive-fiber process, discussed in subsection 3.4.2.2, at 0.85% open area, using 0.0254 cm (0.01 in.) diameter nylon monofilament as the fugitive fiber. Two of the panels were fabricated using 2-ply Narmco Kevlar 49/5209-281 style fabric laminate and designated MFD7100.85K in accordance with the numering system described in subsection 3.4.2.2. The other two panels were fabricated using 3-ply Fiberite HMF134/48A fabric laminates and designated MFD7100.85GW.

4.2 PANEL TESTING

Flow testing of the two types of mechanical property material panels delivered to NASA is described in subsection 3.5.2.2. As noted there, the pressure loss/flow performance of these configurations may be used in all wing areas of the baseline LFC-200-S airplane. The surface smoothness requirements were not met by those panels and further development in this area is required. It is not known whether the hole pattern (paired adjoining holes) would allow satisfactory laminarization.

Six of the perforated composite panels described in subsection 3.4.2.2 were tested for tensile strength and modulus in the 0° (warp), 45°, and 90° (fill) directions. Duplicates of two of these panels, MFD7100.85K and MFD7100.85GW, were delivered to NASA. The other four were MFD7101.2K, MFD7100.85GC, MFD7101.2GC, and MFD7101.2GW. Tensile strength and modulus test results are shown in Table VI for all six perforated composite panels. Typical tensile strength and modulus in the 0° and 90° directions of solid (non-perforated) laminates of the same materials are shown in Table VII. The percentage of solid laminate tensile strength and modulus retained by the perforated composite panels is shown in Table VIII.

TABLE VI - TENSILE PROPERTIES OF POROUS COMPOSITE FACE SHEETS

Specimen	No. of Tests	Orient (Degrees)	Open Area (%)	Tensile Strength		Tensile Modulus	
				MN/m^2	ksi	GN/m^2	MSI
MFD7100.85K	3	0	0.85	373.0	54.1	21.6	3.13
MFD7100.85K	3	45	0.85	61.6	8.93	3.38	0.49
MFD7100.85K	3	90	0.85	270.0	39.2	16.1	2.33
MFD7101.2K	3	0	1.20	325.0	47.1	21.2	3.07
MFD7101.2K	3	45	1.20	63.4	9.2	3.79	0.55
MFD7101.2K	3	90	1.20	212.0	30.7	15.7	2.27
MFD7100.85GW	3	0	0.85	308.0	44.6	47.2	6.85
MFD7100.85GW	3	45	0.85	82.7	12.0	11.7	1.70
MFD7100.85GW	3	90	0.85	166.0	24.1	40.0	5.80
MFD7101.2GW	3	0	1.2	303.0	44.0	44.6	6.47
MFD7101.2GW	3	45	1.2	100.0	14.5	12.6	1.83
MFD7101.2GW	3	90	1.2	170.0	24.6	35.2	5.10
MFD7100.85GC	3	0	0.85	361.0	52.3	50.8	7.37
MFD7100.85GC	3	45	0.85	110.0	16.0	14.0	2.03
MFD7100.85GC	3	90	0.85	263.0	38.2	46.2	6.7
MFD7101.2GC	3	0	1.2	368.0	53.3	47.1	6.83
MFD7101.2GC	3	45	1.2	84.8	12.3	11.5	1.67
MFD7101.2GC	3	90	1.2	181.0	26.3	42.1	6.10

TABLE VII - TENSILE PROPERTIES OF SOLID COMPOSITES

Material	Orient (Degrees)	Tensile Strength		Tensile Modulus	
		MN/m^2	ksi	GN/m^2	MSI
Kevlar 49/934	0	655	95	32.4	4.7
	90	455	66	31.0	4.5
T300/934-133 Style	0	510	74	74.5	10.8
	90	483	70	67.6	9.8
T300/934-134 Style	0	441	64	66.2	9.6
	90	448	65	62.7	9.1

TABLE VIII - PERCENTAGE OF SOLID LAMINATE STRENGTH AND MODULUS

SPECIMEN	ORIENT (DEGREES)	PERCENT OF SOLID LAMINATE	
		STRENGTH	MODULUS
MFD7100.85K	0	57	67
	90	59	52
MFD7101.2K	0	50	65
	90	46.5	50
MFD7100.85GW	0	70	71
	90	37	64
MFD7101.2GW	0	69	67
	90	38	56
MFD7100.85GC	0	71	68
	90	55	68
MFD7101.2GC	0	72	63
	90	38	62

5.0 TASK III - SYMPOSIUM

Lockheed-Georgia Company participated in a symposium at NASA-Langley Research Center on 28 October 1976, along with two other contractors who performed similar programs. Each of the three contractors presented the basics and the results of their respective programs along with recommendations for further work to be performed.

6.0 CONCLUSIONS AND RECOMMENDATIONS

6.1 MATERIALS AND PROCESSES

Microporous composites, fabricated by the resin stage/resin bleed process, were found to possess high porosity of a nature which provides a very lengthy and tortuous flow path.

The fugitive-fiber-process was developed and demonstrated by the production of perforated composite panels. The following further investigations of this process are recommended:

- o To improve the surface smoothness
- o To improve the hole pattern
- o To maintain better control of the hole diameter
- o To improve the fugitive-fiber removal technique

Perforated metal panels were successfully produced by the electron beam process. The hole spacing of these panels was very consistent. However, the hole diameter varied as much as ±20 percent from the nominal, and the hole was found to be tapered, as shown in Figure 27. Further work is recommended on the EB-perforated aluminum panels to better control the hole diameter variation, and to determine the degree of effective protection that can be attained with an anodic coating.

6.2 FLOW PERFORMANCE

In general, all types of materials and processes tested, except for the microporous composites, could be used for the LFC-200-S aircraft (Reference 2).

Flow tests were conducted over a temperature range of 269 to 303°K (25 to 86°F). No effects due strictly to temperature were observed in either $\sigma\Delta P_T$ or friction factor calculations.

The friction factor calculations consolidated all data for electron-beam-perforated and slotted test panels regardless of hole diameter, slot width, material thickness, or percent open area. This should give the basis for determining the pressure loss through the specimen as a function of suction flow, altitude conditions, and the physical properties of the specimen independent of individual specimen testing. However, the empirical friction factor equation, Equation (2), shown on Figure 57, demonstrates the capability of generating a definitive relationship. Due to the data band width in Figure 57, an exact relationship would be difficult to establish; therefore, care should be taken in using Equation (2) in further analyses.

The friction factor, and consequently the pressure loss across a perforated or slotted specimen, is a function of the hole diameter to the fourth power or slot width

to the second power. As illustrated earlier, an error of 10 percent in fabricating the hole diameter (i.e., ±0.0005-inch variation for 0.005-inch hole) of perforated specimens would manifest itself as a 46 percent error in pressure loss. However, the same 10 percent error in manufacturing the slot would only lead to a 21 percent error in pressure loss. Although both appear excessive, the slot manufacturing tolerances are far less stringent than the corresponding tolerances for perforations. However, both appear to present a potential production tolerance problem.

Reference 6 indicates that slots having this tolerance would be marginal while perforations with this tolerance level would be unacceptable. Therefore, it is recommended that further work be carried out in three specific areas to relieve this potential problem:

- Conduct analytical and experimental evaluations to refine the allowable tolerances on suction flow level and distribution for satisfactory laminarization.
- Conduct analytical and experimental evaluations of ducting system configurations designed to relieve the sensitivity of suction flow to suction surface production tolerances.
- Conduct further experimental and development work to improve production control of tolerances in the manufacturing of suction surfaces.

The tendency of the friction factor curves to "flatten out" at lower values of β should be analyzed further to accurately determine the cause and effect of this phenomenon, and develop techniques for its prediction.

The limited contamination studies conducted indicate that a combination of dust and moisture contaminants is more difficult to clean than the others investigated. Further work is recommended to establish efficient cleaning methods for all types of contaminants.

6.3 MECHANICAL PROPERTIES

As shown in Table VIII, the perforated composites retained from 57 to 72 percent of the solid laminate 0° tensile strength and from 63 to 71 percent of the solid laminate 0° tensile modulus. These properties are considerably above the mechanical property requirements stated in Section 3.3.

The mechanical property effect on perforated metals and slotted panels should be determined and documented for design use.

APPENDIX A

RELATIONSHIP BETWEEN SI UNITS AND U. S. CUSTOMARY UNITS

BASIC SI UNITS		
Physical Concept	Measurement	Abbreviation
Length, Altitude	meter	m
Mass	kilogram	kg
Time	second	s
Pressure	Newtons/m^2	N/m^2
Speed	Mach	M
Thermodynamic Temperature	degree Kelvin	^oK
Density	kilograms/m^3	kg/m^3

PREFIXES		
Factor By Which Unit Is Multiplied	Prefix	Symbol
10^9	giga	G
10^6	mega	M
10^3	kilo	k
10^2	hecto	h
10	deca	da
10^{-1}	deci	d
10^{-2}	centi	c
10^{-3}	milli	m
10^{-6}	micro	μ

APPENDIX A (Continued)

CONVERSION FACTORS		
To Convert From	To	Multiply By
^{o}C	^{o}K	$t_K = t_C + 273.15$
^{o}F	^{o}K	$t_K = (5/9)\ (t_F + 459.67)$
foot	meter	3.048×10^{-1}
inch	meter	2.54×10^{-2}
pound mass (lbm avoir.)	kilogram	4.536×10^{-1}
pound force (lbf)	Newton	4.44832
lbm/in^3	kg/m^3	2.768×10^{4}
psi	$Newtons/m^2$	6.895×10^{3}
$lbm/min\ ft^2$	$kg/sec\ m^2$	8.137×10^{-2}
lbm/min ft	kg/sec m	2.475×10^{-2}

APPENDIX B

FLOW TEST EQUIPMENT

The following test equipment was used in conducting the flow tests described herein:

- Mercury manometer:
  Range: 0-36 in.
  Graduations: 0.1 in. of Hg
  Tolerance: ±0.05 in. of Hg
- Oil manometer:
  Range: 0-36 in.
  Graduations: 0.1 in. of Hg
  Tolerance: ±0.05 in. of Hg
- Flowmeter:
  Range: 0-100% Flow (0-9.0 indicated SCFM)
  Graduation: 1.0%
  Tolerance: ±0.5% (+3% meter)
- Thermometer:
  Graduation: 2°F
  Tolerance: ±1°F
- Vacuum pump:
  Setting: Approximately 20 liters/min.
- Wet test meter:
  Graduation: 0.01 liter
  Tolerance: ±0.005 liter

REFERENCES

1. Kosin, R. E., et al: Laminar Flow Control Demonstration Final Report, LFC Design Data. NORAIR Report NOR-61-141, April 1964.

2. Sturgeon, R. F., et al: Study of the Application of Advanced Technologies to Laminar-Flow Control Systems for Subsonic Transports. NASA CR-133949, Lockheed-Georgia Company, May 1976.

3. Braslow, A. L. and Knox, E. C.: Simplified Method for Determination of Critical Height of Distributed Roughness Particles for Boundary-Layer Transition at Mach Numbers from 0 to 5. NACA TN 4363, September 1958.

4. Braslow, A. L. and von Doenhoff, A. E.: The Effect of Distributed Surface Roughness on Laminar Flow. Boundary Layer and Flow Control, Vol. 2, G. V. Lachmann, ed., Pergamon Press, 1961, pp. 657-681.

5. Langhaar, H. L.: Steady Flow in the Transition Length of a Straight Tube. Journal of Applied Mechanics, June 1942, p. A55.

6. Whites, R. C., Sudderth, R. W., and Wheldon, W. G.: Flight Test Results of The Laminar Flow Control X-21 Airplane. Astronautics and Aeronautics, July 1966.